A psychophysical signature of Y-like neuronal responses in human vision

Ana Leticia Ramirez Hernandez

Integrated Program in Neuroscience

by McGill University, Montreal

April, 2021

"A thesis submitted to McGill University in partial fulfillment of the requirements of the degree of Master's (M.Sc.) Integrated Program in Neuroscience"

ACKNOWLEDGEMENTS

I would like to begin by thanking my supervisor, Dr. Curtis Baker for his infinite patience and generosity throughout this master's degree. The scope of this project and my desire to continue a career in research would never have been possible without having as an example a great teacher who stands out for his excellence, and his love for research and teaching.

I would also like to thank Dr. Ari Rosenberg who is an important part in the inspiration and development of this work, and who collaborated remotely to make my master's project happen. I also thank the members of my committee, Dr. Frederick Kingdom and Dr. Leonard Levin, who were always willing to help with their invaluable knowledge and expertise, and who guided me in the best way from the beginning of this master's degree. I also thank Dr. Chang'an Zhan who offered invaluable help to solve technical difficulties, and who collaborated in the set up of my project; to Dr. Liang Zhen for helping to set up and lending the "videoswitcher" used for my psychophysics experiments; to Dr. Omar Cruz Correa for his guidance in statistics and to M.Sc. Sébastien Proulx for his great help in french translations. I also want to thank everyone at McGill Vision Research for providing us with a great environment for learning.

I feel grateful for having such a great family that supports my goals and is my inspiration for continuing to prepare every day. I especially thank my husband Kevin Spears, who has always put my dreams in front of his and has given me unconditional support along this master's.

ABSTRACT

Retinal ganglion cells (RGCs) are the sole output neurons of the retina, conveying visual information to the brain. There are many different types of RGCs, but their possible roles in visual perception are not well understood. In cats, three major types of RGCs have been defined, neurophysiologically (X, Y and W) and morphologically (alpha, beta and gamma/delta, respectively). Y-alpha cells are cat RGCs with a large cell body and large dendritic fields, similar to parasol cells in primates. They project to the LGN, which relays to the visual cortex, and respond linearly or nonlinearly depending on the visual stimuli. The linear response occurs when drifting gratings at low spatial frequencies (SFs) are presented. However, when contrast-reversing gratings at high spatial frequencies are presented, Y-alpha cells respond nonlinearly at twice the temporal frequency of the grating, and at all spatial phases (phase invariance). This particular behavior in cat Y-alpha cells is often referred to as a "Y-cell signature", and is thought to arise from the activation of nonlinear ON and OFF bipolar cells.

Recent neurophysiology studies in primates have found that parasol cells and at least another type of RGC (the smooth-upsilon cell) are not only morphologically similar to cat Y-alpha cells, but also share their characteristic spatial frequency dependent linear and nonlinear responses. Here we will refer to these as Y-like cells, being the primate counterpart of the cat Y-alpha cell. This thesis attempts to create a bridge between the existing neurophysiological evidence for Y-like cells and their behavioral function in humans by developing a psychophysical task that selectively reflects Y-like cell nonlinear properties.

We employed Contrast Modulation (CM) patterns which consist of a high spatial frequency sinewave grating carrier, whose contrast is modulated by a low spatial frequency sinewave envelope. CM patterns with carrier at high spatiotemporal frequencies have been used in cat neurophysiology studies to produce nonlinear ("second order") responses in visual cortex (area 18) and lateral geniculate nucleus (LGN). These responses are likely driven by retinal Y-like cells, that project to the LGN and then to the visual cortex. Here we describe a human psychophysical study that employed CM patterns presented at varying values of spatial frequency, temporal frequency, and eccentricities in the visual field. For comparison, simple luminance modulation (LM) gratings were similarly tested. The psychophysical task was to report the perceived direction of motion of LM gratings or CM envelopes. We found that the ability to correctly perceive direction of motion with CM patterns was bandpass with carrier SF, showing the best performance at high spatiotemporal frequencies. Furthermore, for CM patterns the good performance was rather independent of eccentricity. In contrast, for LM patterns the best performance at high spatial frequencies was at low temporal frequencies, and the performance decreased systematically with eccentricity.

Since the nonlinear subunits of Y-like cells respond better at higher spatial and temporal frequencies than linear mechanisms respond to gratings, the responses are likely driven by nonlinear subunits of Y-like cells. These findings suggest this or similar stimuli and tasks could open up new lines of investigation for selective activation of central neural pathways in the visual system, as well as for the assessment of Y-like cell involvement in clinical conditions such as optic neuropathies.

ABRÉGÉ

Les cellules ganglionnaires rétiniennes (CGRs) sont les seuls neurones permettant d'acheminer l'information visuelle de la rétine au cerveau. Plusieurs types de CGRs ont été identifiés, mais leur rôle dans la perception visuelle demeure méconnu. On retrouve chez le chat trois types majeurs de CGRs, définis selon leur neurophysiologie (X, Y and W) et leur morphologie (alpha, beta and gamma/delta, respectivement). Les CGRs de type Y-alpha du chat ont un large corps cellulaire et arborescence dendritique, similairement aux cellules parasols du primate. Ils projettent au noyau géniculé latéral (NGL) qui fait le relai vers le cortex visuel, et ils répondent de façon linéaire ou non-linéaire selon le type de stimuli visuel. Une réponse linéaire survient à la présentation de grilles dérivantes de basses fréquences spatiales. Des grilles à inversion de contraste de hautes fréquences spatiales évoquent plutôt une réponse non-linéaire au double de la fréquence temporelle du stimulus et peu importe sa phase (invariance de phase). Ce patron de réponse des cellules Y-alpha du chat est souvent considéré comme la "signature des cellules Y", et est compris comme résultant de l'activation des cellules bipolaires ON et OFF.

Des études neurophysiologiques récentes chez le primate montrent que les cellules parasols et au moins un autre type de CGRs (les cellules lisses-upsilon) sont non seulement morphologiquement similaire aux cellules Y-alpha du chat, mais démontrent la même réponse caractéristiquement linéaire ou non-linéaire selon fréquence spatiale. Ici nous désigneront les cellules lisses-upsilon du primate de cellules équivalent Y, en référence à leur homologue chez le chat. Cette thèse vise à faire le lien entre les preuves neurophysiologiques de l'existence de cellules équivalent Y chez l'humain et leur fonction

comportementale en développant une tâche psychophysique qui reflète spécifiquement les propriétés non-linéaires des cellules équivalent Y.

Nous avons utilisé des patrons visuels en Modulation de Contraste (MC) constitués d'une haute fréquence spatiale porteuse dont le contraste est modulé par une enveloppe sinusoïdale de base fréquence spatiale. Des patrons en MC à hautes fréquences spatiotemporelles porteuses ont été utilisé dans des études neurophysiologiques chez le chat pour produire des réponses non-linéaires ("de second ordre") dans le cortex visuel (aire 18) et le NGL. Ces réponses résultent plausiblement de l'action des cellules équivalent Y de la rétine via leurs projections relayées au cortex via le NGL. Ici nous décrivons une étude psychophysique chez l'humain qui utilise des patrons en MC présentés à différentes fréquences spatiales, fréquences temporelles et excentricités dans le champ visuel. Pour fins de comparaison, de simples grilles en modulation de luminance (ML) ont aussi été testées. La tâche psychophysique était de rapporter la direction perçue du mouvement de la grille en ML ou de l'enveloppe de MC. Nous avons observé que la capacité à correctement percevoir la direction du mouvement avec des patrons en MC est de type bande passante selon la fréquence spatiale porteuse, montrant la meilleure performance à haute fréquence spatiotemporelle. De plus, pour les patrons en MC, cette bonne performance s'avère relativement indépendante de l'excentricité. À l'opposé, pour les patrons en ML, la performance à hautes fréquences spatiales était la meilleure à base fréquence temporelle et diminuait avec à plus grande excentricité.

Les sous-unités non-linéaires des cellules équivalent Y répondent mieux aux fréquences spatiales et temporelles hautes que ne le peuvent les mécanismes linéaires en réponse à des grilles. Les performances mesurées ici pour les stimuli en MC de hautes fréquences spatio-temporelles sont donc probablement supportées par des sous-unités non-

linéaires des cellules équivalent Y. Ces résultats suggèrent que notre tâche et stimuli, ou d'autres similaires, pourrait ouvrir une nouvelle voie d'investigation pour une activation sélective des voies neurales centrales dans le système visuel, de même que pour l'évaluation de l'implication des cellules équivalent Y dans des conditions cliniques telles que les neuropathies optiques.

Contributions of the Authors

All of the work presented here was developed under the supervision of Dr. Curtis Baker. The study shown in Chapter 2 was conceptualized by Dr. Baker and Dr. Ari Rosenberg, and the experimental design of this study was a collaboration between Dr. Baker, Dr. Rosenberg, and myself.

The programs for running the experiments were created by Dr. Baker and the code to run the Videoswitcher was adapted by Dr. Liang Zhen. I adapted some scripts from the original work of Dr. Baker, in order to produce different visual stimuli for contrast modulation (CM) and luminance modulation (LM) experiments.

I was responsible for running all the experiments (pilots and finals). I wrote the general introduction (Chapter 1) and the general discussion (Chapter 3) by myself, with the supervision of Dr. Baker. For chapter 2, I was the main responsable for writing the manuscript, with the assistance of Dr. Baker for revising all the sections of the paper and Dr. Rosenberg for revising the Methods section.

Dr. Baker provided the facilities and the equipment necessary to develope this work, and is the holder of the NSERC grant that supported this research.

TABLE OF CONTENTS

LIST OF FIGURES

1 Introduction

Cats have retinal ganglion cells (RGCs) that are similar to those in primates which have been neurophysiologically characterized in three different types known as X, Y, and W cells (Enroth-Cugell and Robson, 1966; Lennie, 1980; Hochstein and Shapley, 1976; Rodieck, 1979; Stone et al., 1979). Morphologically, Y cells correspond to alpha cells that are RGCs with a large cell body and large dendritic fields; X cells correspond to beta cells that have medium size somas and smaller dendritic fields (Boycott and Wässle, 1974), and W cells correspond to gamma and delta cells which have various morphological types with variations in soma, axon and dendritic field size (Fukuda et al., 1985). While X-beta cells are similar to primate midget cells, Y-alpha cells have common properties with parasol cells. Y-alpha cells are a particular subset of RGCs which respond linearly or nonlinearly depending on the visual stimuli. When drifting gratings at low spatiotemporal frequencies are presented, they respond linearly. However when contrast-reversing gratings at high spatiotemporal frequencies are presented, they respond nonlinearly at twice the temporal frequency of the grating, and at all spatial phases (phase invariance). This particular behavior in cat Y-alpha cells is known as the "Y-cell signature", and arises from the activation of nonlinear ON and OFF bipolar cells. Y-alpha cells which we will refer here as Y-like cells possibly exist in most mammals and according to some evidence, they might be predominantly affected in different neurodegenerative diseases, including glaucoma (Shou et al., 2003). The objective of this thesis is to explore the behavior of Y-like cells in terms of human psychophysics, and search for possible approaches to selectively reflect Y-like cells functionality.

In this chapter, we review the neural elements of the retina with a special focus on retinal ganglion cells (RGCs). We discuss the linear and nonlinear properties of the cat Y-alpha RGCs as well as their primate counterpart (parasol, smooth-upsilon cells). We continue with an introduction of first and second-order stimuli, such as contrast modulation (CM) patterns. We discuss the relationship between CM patterns and nonlinear processing of this type of second-order stimuli, likely driven by Y-like cells. We finish this chapter discussing the importance of avoiding display screen nonlinearities and performing a careful calibration of a CRT monitor when using second-order stimuli.

1.1 Neural elements of the retina

Historically, different cultures have described the eyes as “the mirror of the soul” or “the interpreter of the mind”. This might come from observations from the retina, which is the posterior part of the eye and the only element of the central nervous system (CNS) accessible directly from the outside, giving an amazing window to explore the human body.

The retina contains millions of neurons in charge of capturing, transforming, and organizing information that travels from the eye to the brain. Like other CNS structures, it comprises a neural circuit to mediate a complex behavior, enabling us to see. The retina is composed of three layers of neuron cell bodies and two layers of synapses. The outer nuclear layer (ONL), contains cell bodies of the photoreceptors which are the rods and cones. The inner counterpart of this layer, the inner nuclear layer (INL) contains cell bodies of bipolar cells and interneurons which are the horizontal and the amacrine cells. The last layer is called the ganglion cell layer and contains the cell bodies of the retinal ganglion cells (RGCs). The different neuron cell bodies connect to each other through two layers of synapses know as the outer plexiform layer (OPL) and the inner plexiform layer (IPL). The INL contains the amacrine cells, with the horizontal cells outside of this layer, beside of their plexiform connections. The plexiform connections are found in the OPL (at each side of the INL). Here, the nuclear layer synapses with the photoreceptors and the ganglion cell layer. Therefore, rods and cones connect to bipolar and horizontal cells in the OPL. On the other hand, the bipolar cells and amacrine cells of the INL synapse with the ganglion cells in the IPL (Yanoff & Duker, 2019).

In the next sections, we will describe the major classes of retinal neurons and the interactions between them. We continue with the characterization of the retinal ganglion cells (RGCs), the subtypes of RGCs, and classic psychophysical experiments that have determined the role of each type of these neurons in visual processing.

1.1.1 Major retinal neurons and their interactions

The mammalian retina contains more than 50 types of different neurons with diverse functions (Masland, 2001). However, five types of these neurons are recognized as major classes: photoreceptors, horizontal cells, amacrine cells, bipolar cells, and retinal ganglion cells (RGCs) (Purves et al., 2001).

The interactions of neurons in the retina follow a three neuron chain basis allowing the connection between photoreceptors, bipolar cells, and ganglion cells (Purves, Augustine, and Fitzpatrick, 2001). In this regard, the bipolar cells receive information from photoreceptors and transmit these signals to the inner layers of the retina. The interneurons (horizontal and amacrine cells) mediate lateral interactions from the outer layers and the inner layers of the retina, respectively. Finally, the RGCs receive information from bipolar and amacrine cells, and their axons form the optic nerve which communicates the retina with the brain (Gregg et al., 2013). In the next paragraphs, we will discuss in more detail about each of these neurons.

The photoreceptors are light-sensitive neurons. They are the first element for processing vision and are divided into rods and cones. The human retina contains about 120 million rods and 6 million cones. Cones are mostly concentrated in the center of the retina

(fovea) while rods are distributed in most of the retina, except in the central part of the fovea. Rods are neurons with high sensitivity to light, responding to changes in dim light (scotopic vision). Opposite to rods, cones are in charge of photopic vision, functioning at higher levels of light, and are sensitive to color. Both types of photoreceptors have similar structures: outer segment, connecting cilium, inner segment, nuclear region, and synaptic region. In the outer segment, phototransduction occurs which is a process by which light is converted into electrical signals. The connecting cilium connects to the inner segment which contains the organelles of the photoreceptor. The photoreceptor has a synaptic connection, utilizing glutamate as the neurotransmitter, onto bipolar cells (Molday and Moritz, 2015).

Horizontal cells and amacrine cells are retinal interneurons that mediate lateral interactions between photoreceptors and bipolar cells in the OPL, and from bipolar cells to RGCs in the IPL. Amacrine cells have multiple connectivities - they synapse (back) to the bipolar cells, as well as to RGCs, and to other amacrine cells (Masland, 2012). In rabbits, some amacrine cells are thought to mediate direction selectivity in many RGCs (Barlow and Levick, 1965; Yoshida et al., 2001; Amthor et al., 2002), though such direction selectivity is much less evident in higher mammals. Horizontal cells facilitate interactions between photoreceptors, mediating functions such as adjustment of contrast and color opponency (Twig et al., 2003).

The bipolar cells provide a straight pathway to connect photoreceptors and RGCs. Their receptive fields can be either ON-center or OFF-center. ON-center bipolar cells depolarize when light stimulates the center of the receptive field while OFF-center, hyperpolarize when light stimulates the center (Werblin and Dowling, 1969). Some bipolar cells are selective in their synapic connections for a specific type of photoreceptor or even further, for a specific type of cone, while other bipolar cells are not selective being called

"diffuse", receiving mixed inputs. This selectivity is consistent with the extent of the dendritic field of the bipolar axon. In primates, according to the dendritic field, bipolar cells are subclassified as midget-bipolar and diffuse-bipolar. Midget-bipolar cells make contact with a single cone and diffuse-bipolar cells make contact with multiple cones. Both midget-bipolar and diffuse-bipolar cell axon terminals are located in the inner plexiform layer (IPL) (Boycott and Wasle, 1991). In the IPL, ON-center bipolar cells express metabotropic (mGluR) glutamate receptors and react to glutamate by hyperpolarizing their membrane, while OFF-center bipolar cells express ionotropic (iGluR) glutamate receptors and react to glutamate by depolarizing their membrane. These differences in the photoreceptor-bipolar synapse allow different properties in signal transduction (Nelson & Connaughton, 2007). Since bipolar cells are the input neurons of the RGCs, they have been found to be involved in linear and nonlinear mechanisms of a special type of RGC, the Y-like cell. In sections 1.1.2 and 1.2.3 we will discuss further RGCs and Y-like cells.

In the next section "Characterization of retinal ganglion cells" we will discuss further the different types of RGCs, their psychophysical responses to visual stimuli, and the receptive field organization of midget and parasol cells across the retina.

1.1.2 Characterization of retinal ganglion cells

RGCs are the final output of the retina, from where they project to the lateral geniculate nucleus (LGN) and the visual cortex (Wensel TG, 2012). Although more than 18 different morphological types of RGCs in the primate retina have been found (Kolb H et al.,

2001), three main classes with different morphology and function that correspond to parasol cells, midget cells, and small bistratified cells (Rodieck, 1991; Dacey & Lee, 1994) are the most well-characterized. Parasol cells project to magnocellular layers of the LGN and form the magnocellular pathway, midget cells project to parvocellular layers of the dorsal LGN and form the parvocellular pathway, and small bistratified cells project to koniocellular layers and form the koniocellular pathway (Shapley and Perry, 1986; Rodieck, 1991; Dacey & Lee, 1994).

The koniocellular pathway consists of small bistratified cells also known as blue-ON/yellow-OFF (Dacey and Packer, 2003; Dacey et al.,2003, 2005) RGCs which are neurons with small bodies that contribute to blue-yellow color vision (Martin et al.,1997; Szmajda et al.,2006; Chatterjee and Callaway, 2003). The magnocellular pathway includes larger neurons with large dendritic fields and large axons. They form the dominant input to cortical pathways for motion perception (Szmajda, et al., 2005), have larger non-color-opponent receptive fields (ON or OFF center), and high contrast and temporal sensitivity (Kaplan and Shapley, 1982; Leventhal et al., 1981; Perry et al., 1984). Lesions, induced by neurotoxins in the magnocellular pathway, decrease the contrast sensitivity for visual stimuli at high temporal frequencies (TFs) and low SFs (Merigan et al 1991 a). The parvocellular pathway comprises an abundant number of midget cells which have compact dendritic fields and small axons (Leventhal et al., 1981; Perry et al., 1984). Midget cells are sensitive to red-green color, have ON or OFF receptive fields, and lower contrast sensitivity (Derrington and Lennie., 1984; Kaplan and Shapley, 1982).

In the macaque central retina, about 80% and 10% of the total of RGCs are midget and parasol cells, respectively. (Perry et al., 1984). However, in macaque and in the human retina, the ratio of the parasol to midget dendritic field size increases toward the fovea with a

midget/parasol cell density ratio of about 3:1 in the peripheral retina, and 30:1 at 3º (1.4mm) of eccentricity. A possible explanation for this is that the density of parasol cells increases slower than the density of midget cells approaching the central retina, while the dendritic overlap remains constant (Dacey & Petersen, 1992).

In the next section, "Y-like cells", we will first summarize classic neurophysiology experiments that described the linear and nonlinear responses of cat Y-alpha cells. Then, we will introduce more recent neurophysiology studies that characterized primate Y-like cells, and we will finish the section describing two different models that propose a similar origin of second harmonic responses in Y-like cells.

1.2 Y-like cells

The receptive field of a visually responsive neuron is defined as the region of the retina (or equivalently, of the visual field that is viewed by the eye) where a cell is excited or inhibited by light. The organization of the receptive fields of RGCs and the LGN in the cat was first described by Kuffler (1952) and Hubel and Wiesel (1961). Receptive fields of the RGCs and the LGN neurons have a defined organization in two different types known as ON and OFF, which are reciprocal. That means, ON cells are excited when light stimulates the center of their receptive field, while OFF cells are excited with dark stimuli in the center of the receptive field. ON and OFF cells form two distinct pathways from the retina to LGN and

visual cortex. However, arriving at the primary visual cortex the two pathways converge (Hubel and Wiesel, 1962; Wilson et al., 1976).

In the next sections, we will discuss the differences between cat Y-alpha cells and X-beta cells, the homologous Y-alpha cell (Y-like cells) in the primate, and we finish by reviewing physiological models that explain the source of the linear and nonlinear responses of the Y-like cells.

1.2.1 Cat Y-alpha cells and X-beta cells

A lot of the basic knowledge of neurophysiology in vision came from examining the properties of the visual system of the cat. In this mammal, three different functional types of RGCs known as X, Y and W cells (Enroth-Cugell and Robson, 1966; Lennie, 1980; Hochstein and Shapley, 1976; Rodieck, 1979; Stone et al., 1979), that morphologically correspond to beta, alpha, and delta or gamma cells, respectively, have been characterized (Boycott and Wässle et al., 1974; Fukuda et al., 1985). X cells are similar to primate midget cells, i.e. they are small and medium size neurons with small dendritic fields, they have slow axonal conduction and project to layers A and A1 of the cat lateral geniculate nucleus (LGN). Y or alpha cells, are similar to primate parasol cells with large dendritic fields, large receptive fields, and fast axonal conduction. They project to layers A, A1 and C of the cat LGN and to the superior colliculus (SC). W cells have various morphological types with variations in soma, axon and dendritic field size (Fukuda et al., 1985). They are heterogeneous in physiological properties and they are not generally well understood. The majority of the

thalamic input to the early visual cortex in the cat is from X and Y cells (Ferster D, 1990; Cleland et al., 1971). Important differences between X and Y cells are their linear and nonlinear responses to drifting and contrast-reversing gratings (Shapley and Perry, 1986). Responses of X cells to either drifting or contrast-reversing sinewave gratings are at the temporal frequency (TF) of modulation of the stimulus. Consistent with this, the X cell response for a contrast-reversing sinewave grating is dependent on the grating's spatial phase - both results indicate the basically linear behavior of X cells. In contrast, the Y cell's response has two different components, the first component is a linear response at the temporal frequency of the stimulus, called the fundamental (first harmonic) or F1, which is similar to the phase-dependent linear response of the X cell. The second component observed in Y cells (second harmonic or F2) is a response to contrast-reversing gratings at twice the temporal frequency of the stimulus, which does not vary with the spatial phase. When first and second harmonic response magnitudes are plotted as a function of spatial frequency, the two curves are shifted in what has been referred to as the "Y cell signature" (Hochstein and Shapley, 1976; Kaplan and Shapley 1982; Shapley and Perry, 1986) (Figure 1-1). This second harmonic response originates from the activation of small nonlinear subunits in the Y-cells, that arise from a distinct class of cone bipolar cell inputs (Demb et al., 1999; Crook et al., 2008). After leaving the retina, axons of Y-cells (like those of X-cells) project to the LGN, and then to the visual cortex.

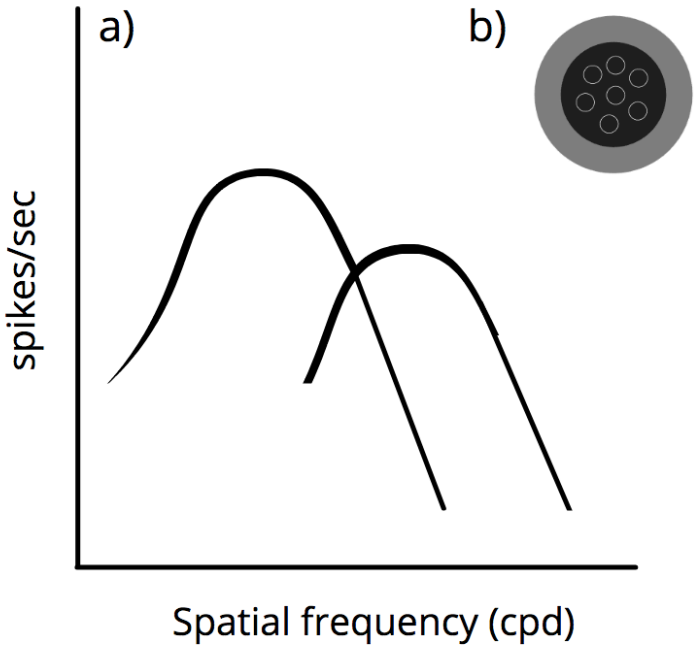

Figure 1-1) a) Inspired by Shapley and Perry (1986). Spatial frequency (SF) responses of cat LGN Y cells. The fundamental curve (F1, first harmonic) represents the linear response of the Y-cat cell at low SFs at the temporal modulation of drifting sinewave gratings. The second curve (F2, second harmonic), represents nonlinear responses at high SFs to contrast-reversing gratings, of the same Y cell. The Y cell second harmonic response (F2) curve crosses the fundamental (F1) response curve at a high spatial frequency (Y-cell signature). b) Inspired from Rosenberg and Talebi (2009). The filled gray circle represents a Y cell, the small circles in the center represent the bipolar cell inputs that activate the nonlinear subunits of the Y-cat cell.

1.2.2 Primate Y-like cells

The existence of a primate counterpart to the cat Y-cell had been debatable until recently when with newer techniques two different studies identified at least two different types

of Y-like cells in macaque monkey RGCs (Crook et al 2008; Petrusca et al., 2007). \\ Crook et al. (2008), using retrograde tracer injections of rodhamine dextran in the superior colliculus (SC) of macaques, demonstrated that parasol cells project via branching axons to both LGN and the SC. For identifying the Y cell signature, once RGCs were labeled and photo stained, they dissected the retina and performed loose cell-attached extracellular recordings with glass microelectrodes while stimulating the receptive fields with different visual stimuli. For identifying linear components of the RGC receptive fields (first harmonic), drifting sinewave gratings at different contrasts and spatiotemporal frequencies were used. For determining nonlinear receptive field properties (second harmonic), they used stationary contrast-reversing gratings systematically shifted in 45º intervals relative to the receptive field midpoint of the cell. In addition to parasol cells, another similar RGC called smooth (SM) cells, which have a smaller soma and axon, but larger dendritic tree and receptive field than parasol cells, also projected to the LGN and to the SC, and were found to have Y-like cell properties. All SM and parasol cells displayed a first and second harmonic in a Y cell signature (Crook et al 2008). Previous to this experiment, Petrusca et al. (2007), by using multielectrode array recordings had found Y-like properties in “upsilon cells”, which are large RGCs with large receptive and dendritic fields (Petrusca et al., 2007) that probably correspond to the "smooth" cells of Crook et al (2008).

1.2.3 Models of Y-like cells

Y-like cells have two excitatory mechanisms. The first excitatory linear mechanism receives inputs from a narrow field. The second excitatory nonlinear mechanism receives inputs from a wider field and processes higher SFs (Enroth-Cugell and Robson, 1966;

Hochstein and Shapley, 1976;), suggesting multiple responses from spatial subunits of the Y-like cell (Hochstein and Shapley, 1976; Derrington et al., 1979). Recordings from bipolar cells from different species (salamander, rabbit, and primate), that express rectification, suggests that the generation of the central nonlinear mechanisms of the Y-like cell which are proportional to contrast might be driven by inputs from the same rectifying bipolar synapse which drives the linear mechanisms (Demb et al., 2001). The voltage of the presynaptic bipolar cells which are rectified at all contrasts might provide nonlinear responses consequent to glutamate release. At high contrast, the output nonlinearity increases the bipolar cell rectification, causing acceleration of the nonlinear response instead of causing saturation, explaining the proportional response to contrast. A potential mechanism for OFF bipolar cell rectification might be the ionotropic glutamate receptor (iGluR) expressed on the bipolar cell dendrites, which enhances transient responses (Demb et al., 2001). Intracellular recordings of ON-center and OFF-center Y-like cells in the guinea pig (Demb et al., 2001) confirmed this assumption, concluding that the linear and the nonlinear mechanisms for the central region of the Y-like cell receptive field, can be driven by the same presynaptic rectified bipolar cells. In this case, OFF bipolar cells provide the excitatory input to the OFF-center Y-like cells and ON-bipolar cells provide the excitatory input for ON-center Y-like cells (Demb et al., 1999).

Demb et al. (2001) propose a model for common bipolar input cell for the central linear and nonlinear responses of the Y-like cell. In this case, for the OFF pathway, when a bar of a high spatial frequency, contrast-reversing grating (e.g. the left one) turns dark, an OFF-center bipolar cell viewing it is stimulated and its membrane potential depolarizes, releasing glutamate at the bipolar-to-ganglion cell synapse. After that, the right bar turns dark, and an adjacent OFF-center bipolar cell depolarizes, increasing its release of glutamate. Thus there are two temporal cycles of glutamate release from the bipolar cells, for each temporal cycle of the

contrast-reversal. The bipolar cell voltage responses are proportional to contrast but are rectified, and there is a second rectification that occurs at the synaptic output (especially at high contrast). The summation of the first and the second OFF-center bipolar cell outputs produces in the Y-like cell a frequency-doubled response. A similar circuit occurs with ON-center bipolar cells, but the output rectification is weaker than that of OFF-center bipolar cells.

The Crook et al. (2008) model is consistent with the rectified signals of the bipolar cells as the input for the second harmonic (F2) of the parasol (Y-like cell), emphasizing the differences between F1 and F2 center receptive fields' estimated radi at different eccentricities. In this model, a spatial array of receptive fields of a group of diffuse bipolar cells provides an input that excites the dendritic field of the parasol cell. The parasol cell responds to contrast-reversing gratings with a nonlinear F2 as a result of combined outputs of these bipolar cells.

Intracellular recordings from a diffuse bipolar cell (Dacey et al., 2000) suggest a rectified response of the parasol cell (Y-like cell) where the responses to light and dark phases of contrast-reversing patterns summate, causing a frequency-doubled response in the Y-like RGC. An important factor in this model is the center diameters of the receptive field of the linear first harmonic (F1), which vary systematically with retinal eccentricity, while F2 diameters are relatively constant across the retina, reflecting a relative constancy of bipolar cell receptive field diameters as a function of eccentricity (Crook et al, 2008).

In the next section, we will introduce the definition of CM patterns and the relevant neurophysiology studies that suggest that CM pattern responses are driven by Y-like cell inputs. We will finish the section by providing an overview of the aims of this thesis.

1.3 First and second order stimuli

The visual system is sensitive to variations in luminance (first-order) stimuli as well as variations in local contrast or texture (second-order or non-Fourier) stimuli. Neurophysiology experiments have demonstrated that neurons in primary and secondary visual cortices can be selective for stimulus orientation, the direction of motion, and spatial frequency (Baker, 1999). In terms of receptive fields, if a receptive field of a V1 simple cell was superimposed on first-order stimulus, light and dark regions of the stimulus would align with excitatory and inhibitory regions of the receptive field, giving a linear response as a product of spatial summation (Baker, 1999). However, second-order stimuli like contrast modulation (CM) patterns composed of high spatial frequency (SF) elements like textures (carrier) that have a coarse variation in contrast (envelope), or spatial offset (for example, illusory contours) have equal amounts of dark and light regions in each receptive field region, producing no net response (Baker, 1999). Therefore, second-order stimuli cannot be processed by simple cells and require additional nonlinear processing. The use of sinewave gratings for the creation of second-order stimuli (such as CM patterns), gives a powerful tool for analyzing neural mechanisms of second-order processing. In the next sections, we will discuss CM patterns and nonlinear responses to CM patterns that are likely driven by Y-like cells. We finish by discussing the importance of avoiding screen nonlinearities and performing an adequate calibration of the CRT screen when using CM patterns.

1.3.1 Contrast modulation stimuli and Y-like cells

Contrast modulation (CM) (Zhou and Baker, 1993, 1994; Li et al, 2014) patterns, which consist of a luminance carrier sine wave grating at high SF whose contrast is modulated by a sine wave envelope at low SF (Fig.1-2a) have been found to drive early visual cortex neurons in cats (Mareschal and Baker, 1998) and macaque monkeys (Li et al, 2014), with selectivity to the carrier orientation and spatial frequency. The carrier selectivity suggests a neural mechanism that is likely driven by nonlinear subunits of Y-like cells, which in cats have been shown to respond to CM stimuli with similar carrier and SF selectivity (Rosenberg et al., 2010; Rosenberg and Issa, 2011). Furthermore, the responses to CM patterns in both LGN (Rosenberg et al. 2010) and area 18 occur at surprisingly high carrier TFs (Rosenberg and Issa 2011; Gharat and Baker, 2012) - this suggests that these responses do not arise from feedback from the visual cortex, and instead probably arise in retinal Y-like cells. These results are consistent with the idea that cortical nonlinear processing of CM patterns is built, ultimately, on inputs from retinal Y-like inputs.

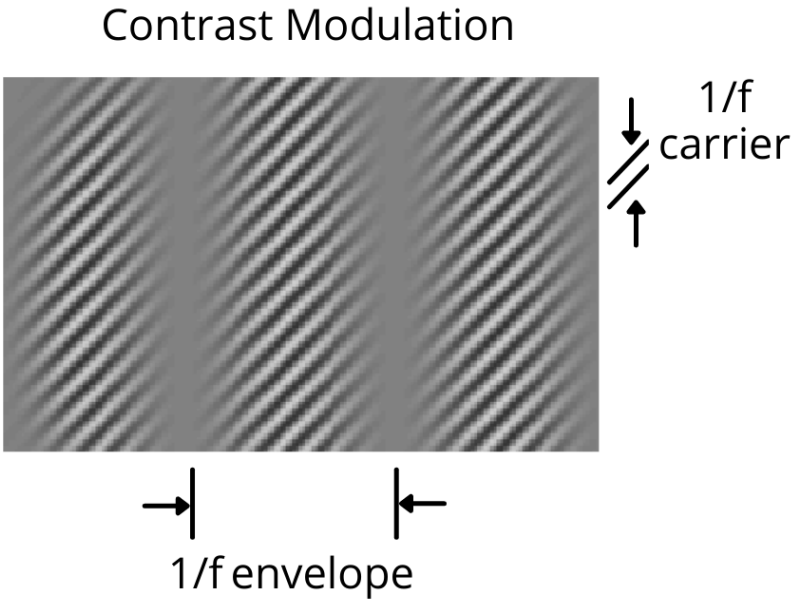

Figure 1-2) Contrast modulation (CM) patterns are a combination of a high spatial frequency grating (carrier) which can have different orientations (in this case it is at 45º), whose contrast is modulated by a low spatial frequency grating (envelope), which here is vertical.

1.3.2 Screen nonlinearities and CM stimuli

In certain vision experiments such as those with second-order stimuli, specifically CM patterns, small screen nonlinearities in the display screen could produce a small distortion resulting in a luminance modulation at the envelope frequency and orientation. For CM stimuli, such nonlinearities can cause a subsequent neural response. Since the contrast threshold for human vision is as low as 0.59 (Blackwell, 1946), such a distortion product in the envelope stimuli close to or higher than this threshold will be noticeable. More generally, any small

nonlinearities early in the visual processing, that might occur by artifacts in the CRT or at the level of the photoreceptors, could cause a minimum difference in the responses to dark-light regions of the carrier, which would produce a very weak signal that could be detected by subsequent linear filtering (Baker, 1999).

However, artifactual distortions introduced by display monitors can be compensated with careful calibration which will be addressed further in the next section of "CRT calibration", and a diffusing sheet that acts as a spatial low-pass filter can be used to make sure that compensation was successful (Zhou & Baker, 1994; Baker 1999; Scott-Samuel & Georgeson, 1999).

1.3.3 CRT calibration for second-order stimuli

The use of computer display systems to show visual stimuli is very common in psychophysics and neurophysiology studies. When using CRT monitors, an accurate calibration to ensure that the displayed luminance levels are known is required (Brainard, 1989). This procedure starts with using a photometer to measure the nonlinear relationship between pixel gray level specified by the computer graphics card and the output luminance on the monitor. Then a descriptive mathematical function is fit to these calibration data, and used as a basis for compensation for the nonlinearity. Otherwise, if such calibration and compensation is not appropriately performed, the influence of the nonlinear voltage (pixel-level) of the display on the luminance gamma function, may affect the content of the images that are being shown (Peli, 1992a). For certain experiments in vision, expanding luminance

resolution in a CRT monitor with a video attenuator that combines the three color outputs of the graphics card is necessary (To L, et al., 2013). For the CRT, a computer controls the content of the video memory of the graphics card where digital to analog converters (DACs) transform the content of video memory in voltage. For color CRT monitors, three DACs (red, green, and blue) are combined to control the luminance of the screen. The bit resolution, defined as the maximum number of voltage levels of a DAC, determines the number of shades of each color. However, the luminance resolution of a display system also depends on the level of noise and the presence of screen nonlinearities (Li et al., 2003). For color monitors, every DAC normally has an 8 bit capacity for generating 256 voltage levels of luminance, or 256 shades of red, 256 shades of green, and 256 shades of blue. In contrast, if the display is set to be monochromatic, the voltages of red, green, and blue have the same voltage, and the system can generate 256 levels of monochromatic luminance (or monochromatic shades) which is insufficient for some visual stimuli used in psychophysics and neurophysiology which require a wider range than 256 luminance levels (Li et al., 2003).

Most visual phenomena are relatively independent of absolute luminance level, and instead depend much more on stimulus contrast (differences in luminance between an object or a point and its background). For example, the standard 8 bit DAC capacity can produce contrast steps of about 0.78% which is too high for some vision experiments. Particularly, when using second-order stimuli, contrast steps of less than 0.03% for monochromatic displays are recommended, with at least 12.7 bits DAC of resolution (Li et al., 2003). This required resolution can be reached by using a resistor network as a video attenuator, which attenuates the outputs of each of the three DACs and re-combines (adds) the attenuated signals in a single analog signal that will drive a monochrome or green gun monitor (Pelli and Zhang, 1991; Li et al., 2003).

The LOBES video switcher (Li et al., 2003) is a video attenuator that modifies the outputs of conventional computer graphics cards to generate high luminance resolution monochromatic displays on color monitors. The video switcher design includes a modified video attenuator (Pelli and Zhang, 1991) whose signal is duplicated by video amplifiers to drive the red, green, blue channels. In theory, the video attenuator for monochrome monitors (Pelli and Zhang, 1991) and the LOBES video switcher are able to generate up to 16 bits of voltage resolution. Of course, factors such as gamma nonlinearities and inaccuracy of graphics card DACs can decrease this number of reachable bits. However, since the recommended number of bits for vision experiments is at least 12.7, these devices give a good secure range to work in vision.

1.4 Organization of the thesis

The general objective of this thesis is to contribute to the knowledge of the functional roles of different types of RGCs. Our hypothesis is that psychophysical performance on an appropriate judgement of CM patterns can reflect the function of Y-like cells. In Chapter 1, we have started with basic retinal anatomy and physiology in order to highlight the neurophysiological variations between the different types of RGCs. We gave an introduction to the cat Y-alpha cells and a review of their linear and nonlinear properties. We also discussed the evidence that supports the existence of analogous primate Y-like RGCs (parasol, smooth-upsilon cells) to which we will refer here as Y-like cells. We continued with a review of first- and second-order stimuli, with special attention to contrast modulation (CM) patterns, which will play an important role in the thesis. We mentioned the importance of avoiding screen nonlinearities and performing a careful calibration of the CRT monitor when using second-order stimuli.

Chapter 2 will be presented in manuscript form appropriate for submission to a journal. In this Chapter, the goal is to selectively activate the nonlinear behavior of Y-like cells using contrast modulation (CM) patterns at high spatiotemporal frequencies and different eccentricities. We use this stimulus in human psychophysical experiments, together with a specific behavioural task, and compare the results with the neurophysiological evidence of Y-like cells described in Chapter 1.

In Chapter 3, we develop a general discussion of the thesis in the context of evidence that suggests selective damage in parasol cells and cat alpha-Y cells in glaucoma, and some caveats regarding this evidence. We discuss the difference between the available tests for

glaucoma detection, and we finish with a section about future directions with respect to the use of CM patterns as a detection test in glaucoma.

2.1 Introduction

Information about the visual world is provided by the retina to the brain only through the responses of retinal ganglion cells (RGCs). There are many different categorically distinct types of RGCs (e.g. Masland, 2001), and establishing the functional contributions of each of the various types of ganglion cells to visual perception has been challenging. In cats, early neurophysiological and morphological studies mainly characterized two different types of RGCs known as X-beta cells and Y-alpha cells (Enroth-Cugell and Robson, 1966; Lennie, 1980; Hochstein & Shapley, 1976) which comprise key elements along the retino-geniculate pathway. Later studies in the primate characterized two main types of RGCs, midget and parasol cells, which were the origin of the parvocellular (P) and magnocellular (M) geniculocortical pathways. Similar to primate midget cells, X-beta cells are compact neurons with small axons and dendritic fields. Y-alpha cells are like primate parasol cells in having large receptive and dendritic fields. Regardless of this apparent correspondence, in early primate studies, it was unclear whether there was a clear primate RGC counterpart of cat Y-alpha cells. Later research demonstrated that parasol cells and at least another type of RGC (smooth/upsilon) that we will refer to here as Y-like cells, exhibit both anatomical and functional properties of cat Y-alpha cells, including their nonlinear responses to visual stimuli (Petrusca et al., 2007; Crook et al., 2008a, b). Despite this evidence clarifying primate Y-like cell properties, the functional role of Y-like cells' nonlinear behavior is not well understood in human visual perception.

According to classic psychophysics experiments, selective lesions in the magnocellular pathway decrease the contrast sensitivity for visual stimuli at high temporal frequencies (TFs)

and low spatial (SFs) but do not affect color vision (Merigan & Manusell, 1990; Schiller et al. 1990; Merigan et al 1991 a). However, these experiments did not address the contributions of the nonlinear responses of Y-like cells. Y-like cells are distinctive neurons: at low spatial frequencies (SFs) they show a linear first Fourier harmonic (F1) response at the temporal frequency of a drifting grating, but when contrast-reversing gratings at high SFs are presented, they display a prominent second Fourier harmonic (F2) nonlinear response. This pattern of SF-dependence of F1 and F2 responses is often referred to as the "Y-cell signature" and is characteristic of the nonlinear summation of Y-like cells (Hochstein and Shapley, 1976). The F1 response is dependent on the spatial phase of a contrast-reversing grating, while the F2 nonlinear response is phase-independent. This characteristic phase invariance of the F2 in the Y-like cell reflects the activation of nonlinear subunits originating from cone bipolar cell inputs (Demb et al., 1999; Crook et al., 2008a, b). In neurophysiology experiments in primates, estimates of the nonlinear center receptive fields (F2) of the Y-like cells, seem to differ from their linear counterparts (F1). While F1 center receptive fields clearly decrease substantially with eccentricity, F2 nonlinear center receptive fields maintain a similar size across a large range of retinal eccentricities (Crook et al., 2008 b).

Contrast modulation (CM) patterns consist of a carrier sine wave grating at high SF, whose contrast is modulated by a sine wave envelope at low SF (Rosenberg et al., 2010; Rosenberg and Issa, 2011). Neurophysiology studies have demonstrated that cortical neurons' responses to CM patterns are critically dependent on subcortical inputs from Y-like cells. The nonlinear subunits of Y-like cells respond to high spatiotemporal frequencies of CM patterns with selectivity to moving carrier patterns (Gharat and Baker, 2017; Rosenberg et al., 2010; Rosenberg and Issa, 2011).

Here, we leveraged the Y-like carrier response properties to CM patterns to create a novel psychophysical approach to reflect the function of Y-like cells. Employing CM patterns with a carrier at high spatial and high temporal frequencies, the carrier is almost perceptually invisible, but it can drive many cortical neurons when an appropriate envelope is imposed on it. Taking into account that the center receptive field of the F2 (nonlinear) Y-like cells vary little with eccentricity (Crook et al, 2008 b), we psychophysically tested our CM stimulus at different spatial and temporal frequencies, and eccentricities, to test whether the pattern of results reflected the selectivity of Y-like cell processing, in comparison to linear mechanisms, as reflected in responses to luminance gratings.

2.2 Methods

Subjects

Four healthy young subjects (aged 23 to 35 years, 2 males, 2 females) participated in the study, one of whom was an author (ARH). The rest were students from McGill University and were naive to the aim of the study. All the subjects had a monocular visual acuity (VA) or best-corrected VA of at least 20/25, and denied any history of ophthalmological diseases or surgeries. All procedures were approved by the Research Ethics Board of the Research Institute of McGill University Health Center. All the subjects gave written informed consent to participate.

Apparatus

Visual stimuli were produced on a Macintosh computer (MacPro 4.1, MacOS X 10.6.8, 2x2.8 GHz Quad-Core, 24 GB RAM) with custom software written in MATLAB (MathWorks, Inc.) using Psychophysics Toolbox, version 3.0.10 (Brainard, 1997; Kleiner et al., 2007; Pelli, 1997). The stimuli were presented on a cathode-ray tube (CRT) monitor (Iiyama, 39.5 cm x 29.5 cm, 120 Hz, 1024 x 768 pixels) at a viewing distance of 221 cm. To achieve linearization and high monochromatic luminance level resolution, we first measured the CRT gamma nonlinearity with a photometer (United Detector Technology S370), and then used the LOBES video switcher (Li et al 2003) that combines blue and attenuated red outputs from the graphics card to generate 16 bits of voltage resolution.

Stimuli

The stimuli were presented at the center of the screen within a cosine-tapered circular window, on a uniform background at the mean luminance of the pattern. We presented both first-order, luminance modulation (LM) gratings as well as second-order, contrast modulation (CM) gratings. The drifting LM gratings were defined by:

$$I(\mathrm{x},\mathrm{y},\mathrm{t})=\mathrm{LB}\{1.0+\mathrm{CLM}\cos(\omega_{\mathrm{SF}}\cdot[\cos(\theta)\cdot\mathrm{x}+\sin(\theta)\cdot\mathrm{y}]-\omega_{\mathrm{T}}\cdot\mathrm{t})\} \quad (1)$$

Here, I (x, y, t) is the luminance intensity of a pixel at spatial location (x, y) at time t, L_B is the background (and mean) luminance, C_{LM} is the Michelson contrast of luminance modulation, ω_{SF} is the spatial frequency, θ is the orientation, and ω_T is the temporal frequency. The sign (positive or negative) of ω_T determined the direction of motion. In these experiments, the orientation was always vertical, so the motion was either leftwards or rightwards.

The CM gratings were defined by sinusoidal modulations of the contrast of a high spatial frequency carrier grating by a low spatial frequency envelope grating (Fig. 2-1a):

$$I(x,y,t) = L\mathrm{B}\,\{\,1.0\; + \mathrm{Carr}(\mathrm{x},\mathrm{y},\mathrm{t}) \cdot [1 + Env(x,y,t)/2]\} \qquad (2)$$

Here, $Env(x,y,t)$ is the envelope pattern, comprised of a drifting grating in the same form as equation 1, with an orientation, spatial frequency, and temporal frequency (direction) that is defined independently of the carrier. L_B represents the background (and mean) luminance. In these experiments, the envelope was always vertical, and drifting leftwards or rightwards.

$\mathrm{Carr}(\mathrm{x},\mathrm{y},\mathrm{t})$ is the carrier pattern, which is a contrast-reversing grating, with an orientation, spatial frequency, and temporal frequency (direction) that are defined independently of the envelope:

$$\mathrm{Carr}(\mathrm{x},\mathrm{y},\mathrm{t}) = \mathrm{Cc}\,\cos(\omega_{\mathrm{Sc}} \cdot [\cos(\theta\mathrm{c}) \cdot \mathrm{x} + \sin(\theta\mathrm{c}) \cdot \mathrm{y}]\,)\;\sin(\omega_{\mathrm{Tc}} \cdot \mathrm{t}) \qquad (3)$$

Here, ω_{Sc} is the carrier spatial frequency, ω_{Tc} is the carrier temporal frequency, θc is the carrier orientation and Cc is the carrier contrast. In these experiments the carrier orientation was always right-oblique, as in Fig 2-1a.

A grey cardboard surround was used to approximately match the mean luminance (L_B) of the CRT stimuli.

Design and experimental procedures

Subjects were instructed to look at a fixation target which was placed at several positions to the upper right of the center of the screen (Fig. 2-1b), such that the stimulus pattern would be presented at 2.1, 4.3, 6.4, or 8.5 degrees of eccentricity in the observer's visual field. On each trial, a stimulus was presented for 250 ms. The perceived direction of motion of the envelope was indicated by pressing a key (Fig 2-1 c), with no time limit, and with subsequent feedback (visual icon on display screen) for incorrect responses. Performance was measured by a method of constant stimuli with seven logarithmically spaced level values of spatial or temporal frequency, all at a fixed value of contrast chosen on the basis on pilot results. A minimum of three blocks of 140 trials, with 20 trials per level, was tested for each condition to provide a total of at least 60 trials per condition with an average time of 5 to 10 minutes per block of trials.

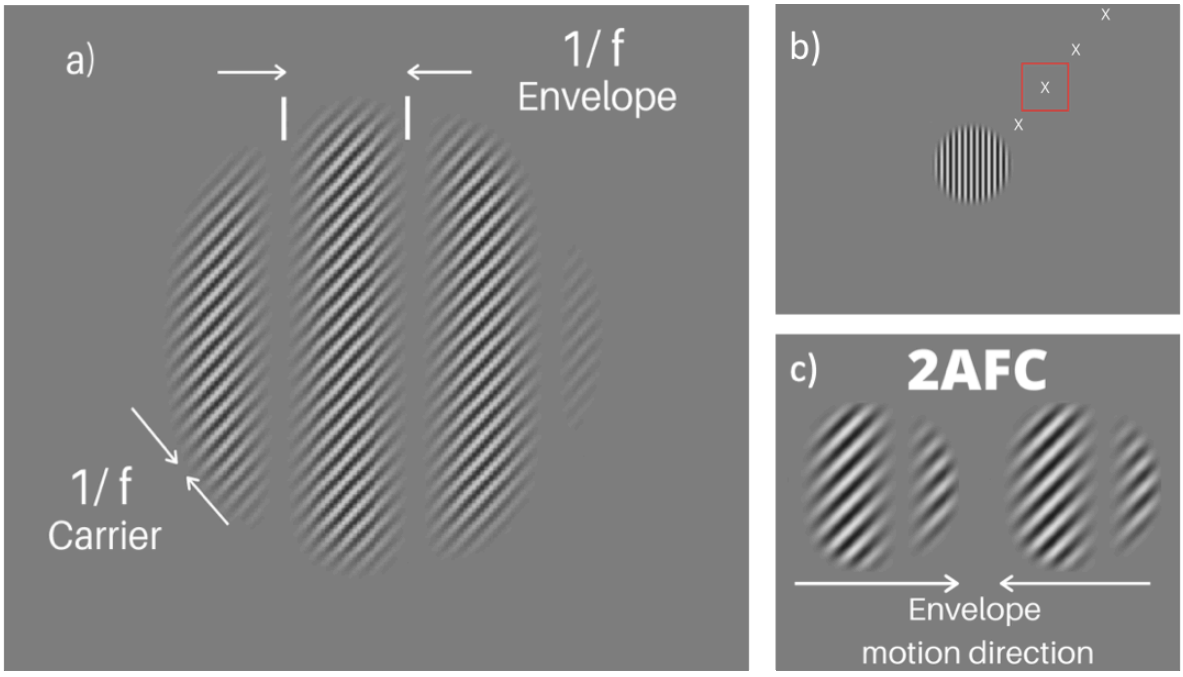

Fig. 2-1. Visual stimuli and psychophysical task. a) Example of contrast modulation (CM) pattern, presented within a cosine-tapered circular window consisting of a high spatial frequency contrast reversing grating (carrier, right-oblique), whose contrast is modulated by a low spatial frequency, vertical sinewave envelope. b) Example of LM stimulus in the center of the screen, and different fixation targets at 2.1, 4.3 (in a red square), 6.4 and 8.5 degrees of eccentricity. c) Depiction of psychophysical task, 2 alternative forced choice (2AFC) in which the subject reports the direction of motion (left vs right) of a CM envelope (shown here) or LM grating. In (a) and (c) the stimulus images are shown at larger than true scale for purposes of illustration.

Data analysis and statistics

For estimating the performance in front of CM and LM patterns, percent correct data from individual subjects were obtained. Standard errors were calculated for each condition, based on the variance of a binomial distribution. For mean responses from all of the subjects (N=4), standard error of the mean was calculated.

In order to determine the highest visible spatial frequency (spatial frequency acuity) from each condition, plots of percent correct data (mean responses from all the subjects) were fitted with a logistic function using a maximum likelihood criterion. For this purpose, only the 5 values on the high-SF roll-off were analyzed, to provide a monotonically decreasing function. Threshold values of maximal carrier SF (for CM) or SF (for LM) were taken at the 75% correct level. The associated standard errors were estimated with bootstrapping. The logistic curve-fitting and bootstrap analysis was performed with routines from the Palamedes Toolbox (Prins & Kingdom, 2018).

2.3 Results

Experiment 1: Spatial frequency dependence at different temporal frequencies

The aim here was to test psychophysical performance on CM patterns with varying values of carrier SF and TF, at a fixed eccentric fixation, to compare to what might be expected if the CM carrier were detected by the nonlinear subunits of Y-like cells. But first, to provide a comparative context for such results, we also made similar measurements for luminance gratings (LM patterns), at the same eccentricity and over the same ranges of spatial and temporal frequency.

In each stimulus presentation of 250 msec duration, an LM or CM pattern was presented in the center of the screen while the subject was fixating a target at 4.3 degrees away from the stimulus (Fig. 2-1b, red square). The psychophysical task was to report the perceived direction of motion of the LM grating or of the CM envelope. Within each block of trials, the LM grating spatial frequency, or CM carrier spatial frequency, was varied with a method of constant stimuli, with a fixed value of temporal frequency (gratings) or carrier temporal frequency (CM envelopes). In separate blocks of trials, the dependence of performance on spatial frequency was measured for different values of temporal frequency (LM), or carrier temporal frequency (CM).

The LM stimuli (vertical gratings, drifting leftwards or rightwards), were presented with a Michelson contrast of 5%. Percent correct performance to report direction of motion as a function of SF is plotted for one subject in Fig. 2-2a, for each of a series of values of

TF. The ability to correctly perceive direction of motion at relatively high SFs (1.5 to 3.0 cpd) occurred only at low TFs (5 to 10 Hz). Note that the fall-off in performance seemed to occur at successively lower SFs, for increasing values of TF. Fig. 2-2b,c,d plot the same kind of results for 3 other subjects, which appeared to show largely similar results, though the results for the two lowest TF values seemed more similar, and the overall interaction was not so evident for the subject in Fig. 2-2d. The average performance, across all 4 subjects, is plotted in Fig. 2-2e. Note again that performance falls off with increasing SF, with a fall-off at lower values of SF for higher TF values. These observations were confirmed with a 2-way ANOVA performed on the average-subject results (Fig 2-2e), showing a significant main effect for SF, $F(6,18)=38.281$, ($p < .001$); a significant main effect for TF $F(3,9)=15.259$, $p < .001$; and a significant interaction effect $F(18,54)=3.841$, $p < .001$.

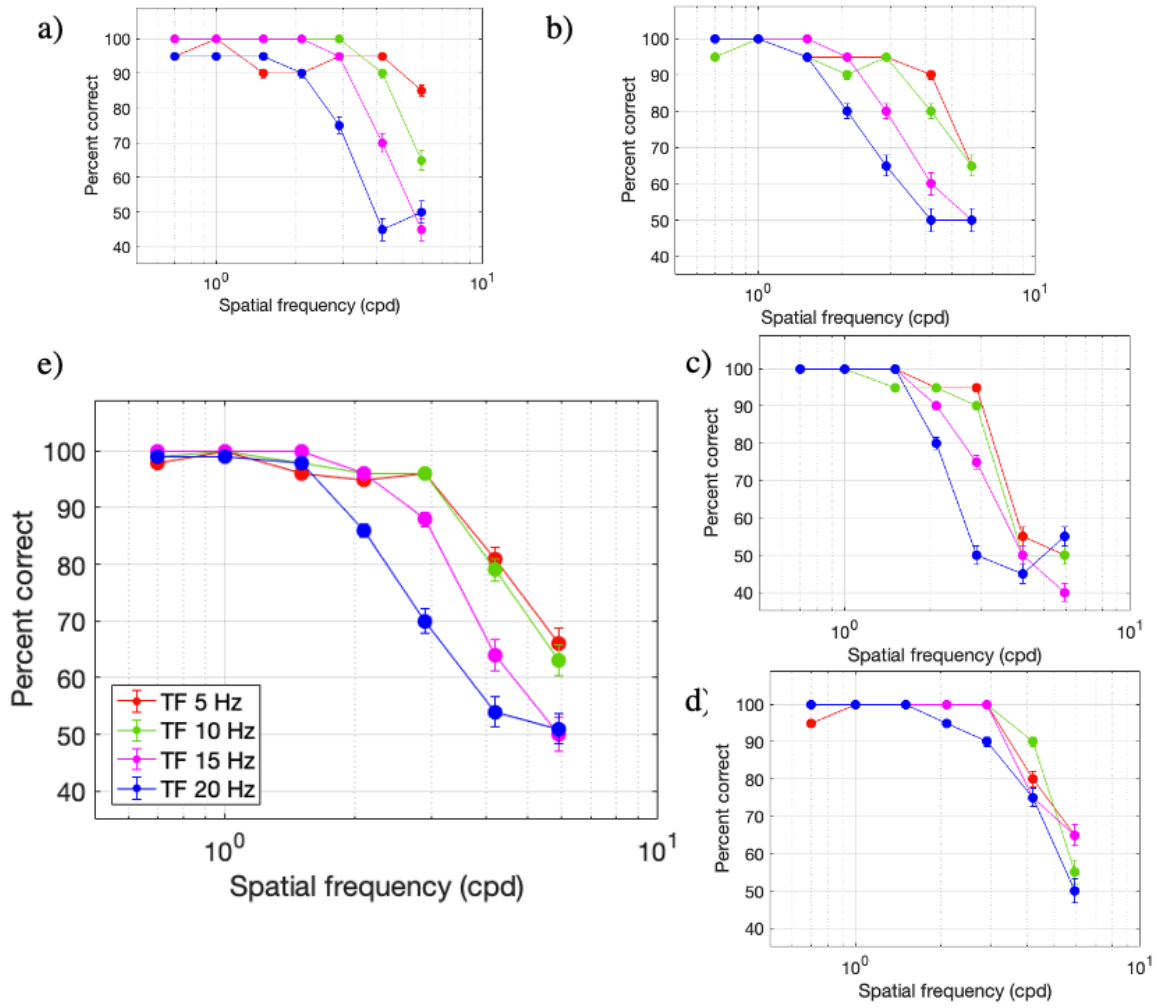

Figure 2-2. Psychophysical performance for luminance modulation (LM) patterns. LM patterns consisted of a drifting grating; the psychophysical task was to discriminate the direction of motion of the grating while fixating monocularly, at 4.3 degrees of eccentricity. The percent correct responses were measured while varying spatial frequency (SF) within trial blocks, for different values of temporal frequency (TF): red, 5Hz; green, 10 Hz; magenta, 15 Hz; blue, 20 Hz. **a-d)** Individual percent correct responses for each of the subjects. **e)** Mean percent correct responses of the four subjects. Error bars represent the binomial standard error (SE) of each condition for each subject **(a-d),** and the SE of the mean (N=4) for subject-averaged results **(e)**.

In general, the performance for LM patterns at relatively high SFs was best at low TFs, and decreased consistently with higher values of SF or TF. This replicates the well-

known psychophysical results for LM patterns as functions of SF and TF in central vision, where performance at high SF was best at low TF, and viceversa (Robson, 1966; Kulikowski, 1970; Watson & Ahumada, 2016).

The CM stimuli had a contrast-reversing grating carrier with right-oblique orientation (45 deg) and a contrast of 80%. The carrier contrast was modulated by a vertical drifting sinewave grating envelope with a modulation depth of 80%, SF of 0.25 cpd, and TF of 3 Hz. Percent correct performance to report direction of envelope motion as a function of carrier SF is plotted for one subject in Fig. 2-3a, for each of a series of values of carrier TF. The ability to correctly perceive direction of motion generally had the best performance at mid-range carrier SFs (1.5 to 3.0 cpd) that were relatively higher than the SFs giving best performance for LM stimuli (Fig 2-2). Another difference from the LM results is that the CM performance at higher SFs was relatively more robust with increasing carrier TF. Fig. 2-3b,c,d plot the same type of data for 3 other subjects, with largely similar results in each case. The average performance across all 4 subjects (Fig. 2-3e) shows a bandpass dependence on carrier SF, which is very similar for different values of carrier TF - the performance at different carrier TFs is very similar, with the curves almost overlapping. These descriptions were confirmed using a 2-way ANOVA, which showed a statistically significant effect of carrier SF, $F(6,18)=88.13$, $p=2.35e-12$ ($p < .001$), but no significant effect of carrier TF $F(3,9)=3.538$, $p=0.061$ or interaction of carrier SF and TF, $F(18,54)=1.352$, $p=0.194$.

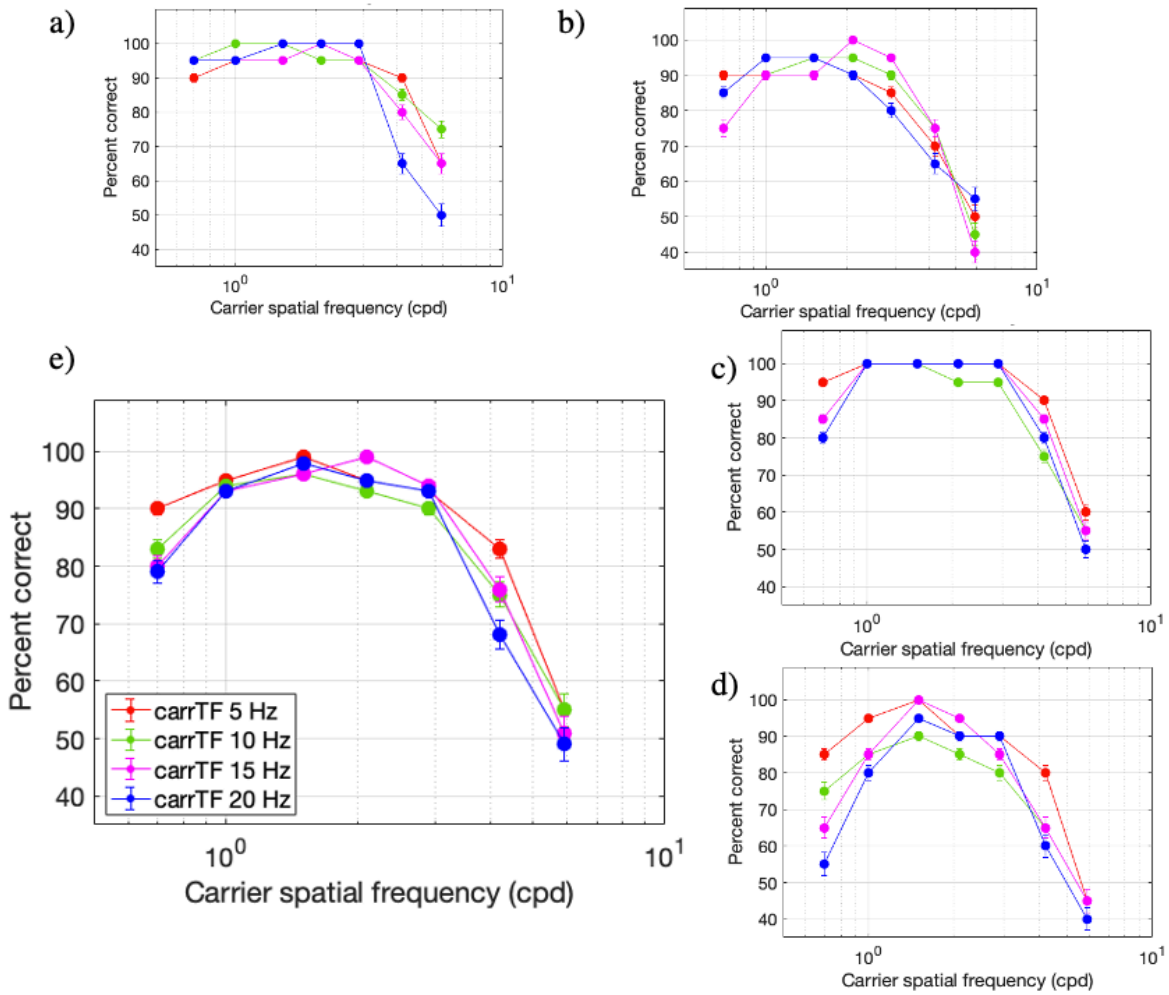

Figure 2-3. Psychophysical performance for contrast modulation (CM) patterns. CM patterns consisted of a contrast-reversing grating (carrier), within a drifting sinewave envelope having a spatial frequency (SF) of 0.25 cycles per degree (cpd) and a temporal frequency (TF) of 3 Hz. The psychophysical task was to discriminate the direction of motion of the envelope while fixating monocularly, at 4.3 degrees of eccentricity. The percent correct responses were measured while varying carrier SF, for different carrier TF values: red, 5Hz; green, 10 Hz; magenta, 15 Hz; blue , 20 Hz. **a-d)** Percent correct responses for each of the individual subjects. **e)** Mean percent correct responses averaged over all the subjects. Error bars represent the binomial standard error (SE) of each condition for each subject **(a-d)**, and the SE of the mean (N=4) for the subject-average response **(e)**.

As a whole, the performance for CM patterns was relatively good at higher carrier SFs and TFs, than seen for LM patterns - and with a large degree of independence between the effects of carrier SF and TF. These results are different than what is expected for LM patterns where psychophysical performance is good only when high SF is combined with low TF or vice versa (Robson, 1966; Kulikowski, 1970; Watson & Ahumada, 2016). In particular, these results for CM patterns (Fig. 2-3) are in contrast to those found for LM stimuli (Fig. 2-2) over the same ranges of spatiotemporal frequencies, consistent with the idea that the carrier processing for CM stimuli is fundamentally different from that for luminance stimuli.

In comparing the results for LM and CM stimuli, the differences in highest SFs giving good performance provided a useful way to quantitatively compare LM and CM performance in a compact manner. Therefore we obtained measures of SF acuity from the data in Figs. 2-2 and 2-3, by using curve-fits to the high-frequency fall-off with SF, and taking the value of SF corresponding to 75% correct as an estimate of SF acuity. The results of this analysis are plotted in Fig. 2-4, showing that SF acuity for LM stimuli (red) declines systematically with TF, while the carrier SF acuity for CM (blue) remains relatively constant with carrier TF. To formally confirm this assessment, we used Pearson correlation coefficients (PCC). For LM patterns, the PCC was $r(2) = -0.9809$, which was significant ($p= 0.0191$) between mean values (N=4) of SF threshold and TF. For CM patterns, the PCC of $r(2) = -0.8211$ did not show a significant correlation ($p=0.1789$) between the mean carrier SF threshold and mean carrier TF (N=4).

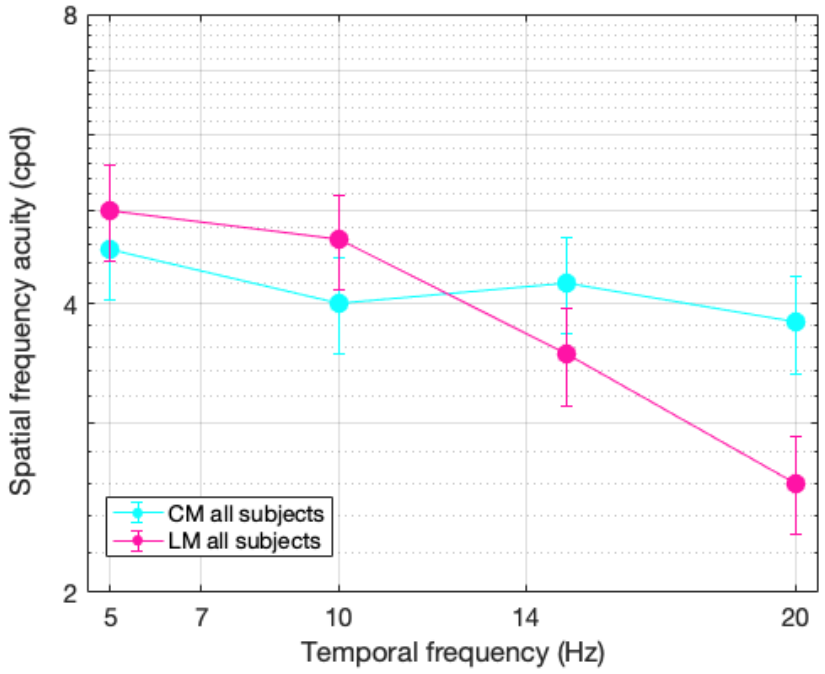

Fig. 2-4. Spatial frequency acuity (i.e. maximal spatial frequency corresponding to 75% correct) obtained through curve-fitting to the high-frequency roll-off of the data in Figs. 2-2e and 2-3e, for LM (cyan) and CM (fuchsia) patterns, respectively. Error bars indicate +/- SE of mean thresholds for the N=4 observers.

Experiment 2: Eccentricity dependence at different temporal frequencies

In order to make a comparison with what could be expected if the CM carrier was detected by nonlinear subunits of Y-like cells, we tested the psychophysical performance in CM patterns with a fixed TF at different levels of retinal eccentricities, in each case as a function of carrier SF. Similar to Experiment 1, we compared the results with those of LM patterns, with the same degrees of retinal eccentricity and SF.

In each stimulus presentation of 250 msec duration, an LM or CM pattern was presented in the center of the screen while the subject was fixating a target at 2.1, 4.3, 6.4, and 8.5 degrees of eccentricity (Fig. 2-1b). The psychophysical task was to report the perceived direction of motion of the LM grating or of the CM envelope. Within each block of trials, the LM grating SF, or CM carrier SF, was varied with a method of constant stimuli, with a fixed value of TF (for LM) or carrier TF (for CM). The dependence of performance on SF or carrier SF was measured at only one value of TF, or carrier TF, respectively of 20 Hz. Different eccentricities were tested in separate trial blocks.

The LM stimuli (vertical drifting gratings, drifting leftwards or rightwards), were presented with a Michelson contrast of 5%. Percent correct performance to report the direction of motion of the grating as a function of SF is plotted for one subject in Fig. 2-5a, for each of a series of eccentricities. We can note that the ability to correctly perceive the direction of motion decreases with SF as well as with eccentricity. Fig. 2-5b, c, d, which represent 3 other individual subjects, show very similar results. The average performance, across all 4 subjects is plotted in Fig. 2-5e where we can note a systematic fall-off in performance at successively higher SFs and eccentricities. These interpretations were confirmed with a 2-way ANOVA performed on the average-subject results (Fig 2-5e), showing a significant main effect for the SF, $F(6,18)=75.664$, $p < .001$; a significant main effect for eccentricity $F(3,9)=10.457$, $p=0.003$; and a significant interaction effect $F(18,54)=4.376$, $p < .001$

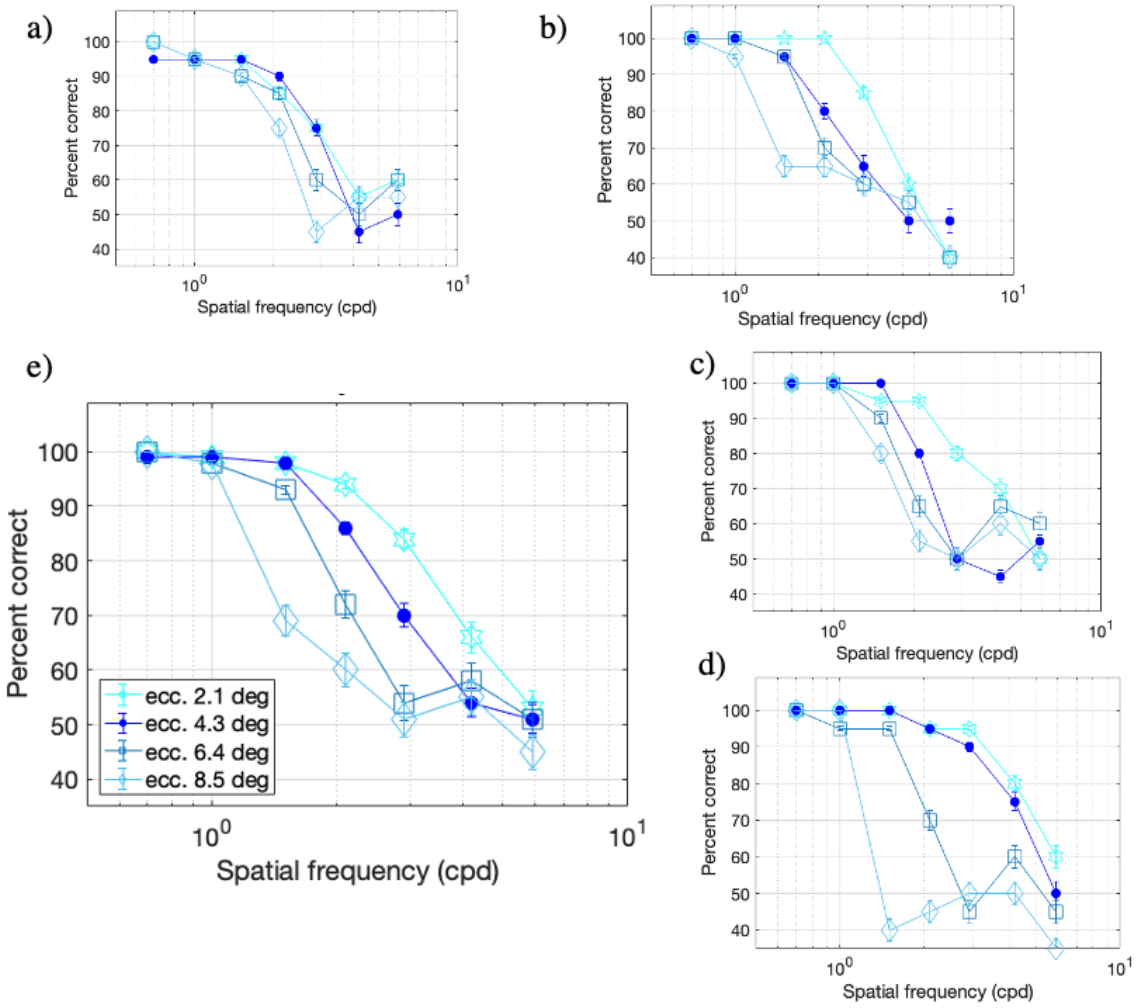

Figure 2-5. Percent correct responses for luminance modulation (LM) drifting gratings at different retinal eccentricities and 20 Hz temporal frequency (TF); the psychophysical task was to discriminate the direction of motion of the grating while fixating monocularly. The percent correct responses were measured while varying spatial frequency (SF) and fixating at different retinal eccentricities (showed in different tones of blue and different symbols): empty hexagrams, fixation at 2.1 deg; filled circles, 4.3 deg; empty squares, 6.4 deg; empty diamonds, 8.5 deg. **a-d)** Individual percent correct responses (for each subject) at each of the different eccentricities. **e)** Mean percent correct responses of the four subjects. Error bars represent the binomial standard error (SE) of each condition for each subject **(a-d)**, and the SE of the mean for subject-averaged results (N=4) **(e)**.

As a rule, the performance for LM patterns decreased systematically with higher SF and larger eccentricity. Important effects on the dependence between SF and eccentricity were observed for all the subjects. These results are consistent with what is expected for LM patterns, where the dependence of contrast sensitivity as a function of SF, shifts to lower SFs as eccentricity increases (Koenderink et al., 1977; Rovamo et al., 1978).

The CM stimuli had a contrast-reversing grating carrier with right-oblique orientation (45 deg) and a contrast of 80%; the carrier contrast was modulated by a vertical drifting sinewave grating envelope with a modulation depth of 80%, SF of 0.25 cpd, and TF of 3 Hz. The carrier contrast was chosen based on preliminary experiments, to provide roughly similar ranges of psychophysical performance as for the LM patterns. Percent correct performance to report the direction of envelope motion as a function of carrier SF is plotted for one subject in Fig. 2-6a, for each of a series of values of eccentricity, at a fixed TF (20 Hz). The ability to correctly perceive envelope direction of motion generally had the best performance at mid-range carrier SFs (1.5 to 3.0 cpd) and seems rather independent of eccentricity compared to the results for LM stimuli (Fig. 2-5). Fig. 2-6b, c, d plot the same type of data for 3 other subjects, with similar results than Fig. 2-6a, though the results for these 3 subjects show a more bandpass dependence on carrier SF compared to Fig 2-6a. The average performance across all 4 subjects (Fig. 2-6e) shows a bandpass dependence on carrier SF with big similarity for different values of eccentricity (with curves almost overlapping). These impressions were confirmed with a 2-way ANOVA of the average-subject results (Fig 2-6e), which showed a significant main effect for the carrier SF, $F(6,18)=20.889$, $p < .001$), but no significant main effect for eccentricity $F(3,9)=3.249$, $p=0.074$ and also not a significant interaction effect $F(18,54)=1.685$, $p=0.072$.

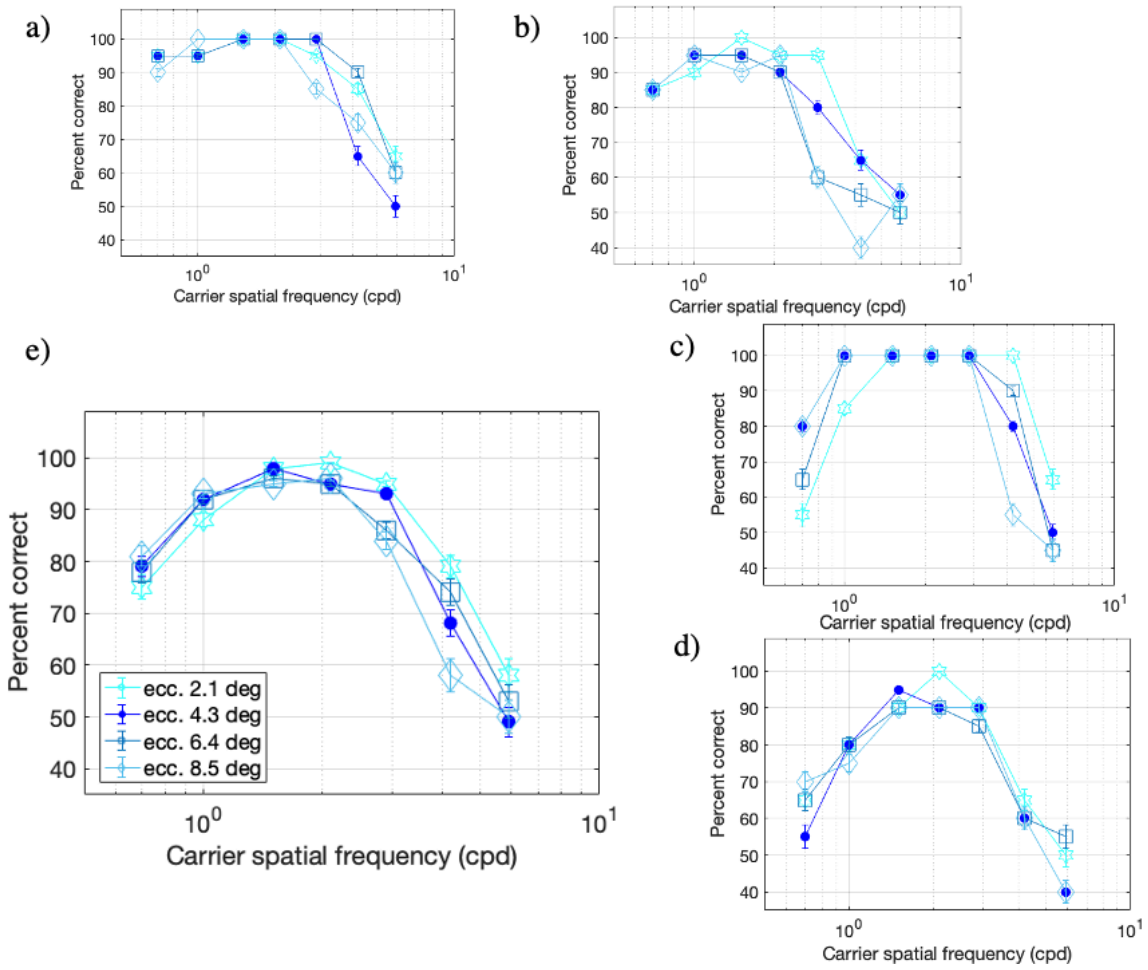

Figure 2-6. Psychophysical performance for contrast modulation (CM) patterns at different retinal eccentricities from fixation. CM patterns consisted of a contrast-reversing grating (carrier), within a drifting sinewave envelope having a spatial frequency (SF) of 0.25 cycles per degree (cpd) and a temporal frequency (TF) of 3 Hz. The psychophysical task was to discriminate the direction of motion of the envelope while fixating monocularly at different degrees of retinal eccentricity: empty hexagrams, fixation at 2.1 deg; filled circles, 4.3 deg; empty squares, 6.4 deg; empty diamonds, 8.5 deg. The percent correct responses were measured while varying carrier spatial frequency, for a fixed carrier TF of 20 Hz. **a-d)** Individual percent correct responses for each of the subjects. **e)** Mean percent correct responses of the four subjects. Error bars represent the binomial standard error (SE) of each condition for each subject **(a-d)** and the SE of the mean for subject-averaged results (N=4) **(e)**.

For the most part, the performance for CM patterns at high fixed TF was good at higher carrier SFs than was seen for LM patterns (Fig. 2-5), and had clear independence of the effects of carrier SF versus eccentricity, contrasting with the results from LM patterns. What is expected for LM patterns, is that the dependence of contrast sensitivity on SF, shifts to lower SFs when increasing eccentricity (Koenderink et al., 1977; Rovamo et al., 1978). However, for CM patterns our results (Fig. 2-6) are relatively independent of eccentricity. To compare, note the difference with the performance for LM stimuli in Fig. 2-5, which is displayed over the same ranges of SF and eccentricity. In particular, these results are consistent with the idea that the processing of CM patterns across eccentricities, is different from that for LM patterns.

Similar to Experiment 1, a practical way to compare LM and CM performance in a concise manner, was to measure the differences in highest SFs giving a good performance. Consequently, we estimated SF acuity from the data in Figs. 2-5 and 2-6, by using curve-fits to the high-frequency fall-off with SF, and taking the value of SF corresponding to 75% correct (threshold). The results of this analysis are plotted in Fig. 2-7, showing that SF acuity for LM stimuli (orange) declines systematically with eccentricity, while the carrier SF acuity for CM (purple) remains relatively constant with eccentricity. To formally confirm this assessment, we used Pearson correlation coefficients (PCC). For LM patterns, the PCC was $r(2) = -0.9915$, which was significant ($p=0.0085$) between mean values ($N=4$) of SF threshold and eccentricity. For CM patterns, the PCC of $r(2) = -0.9487$ did not show a significant correlation ($p=0.0513$) between the mean carrier SF threshold and mean carrier TF ($N=4$).

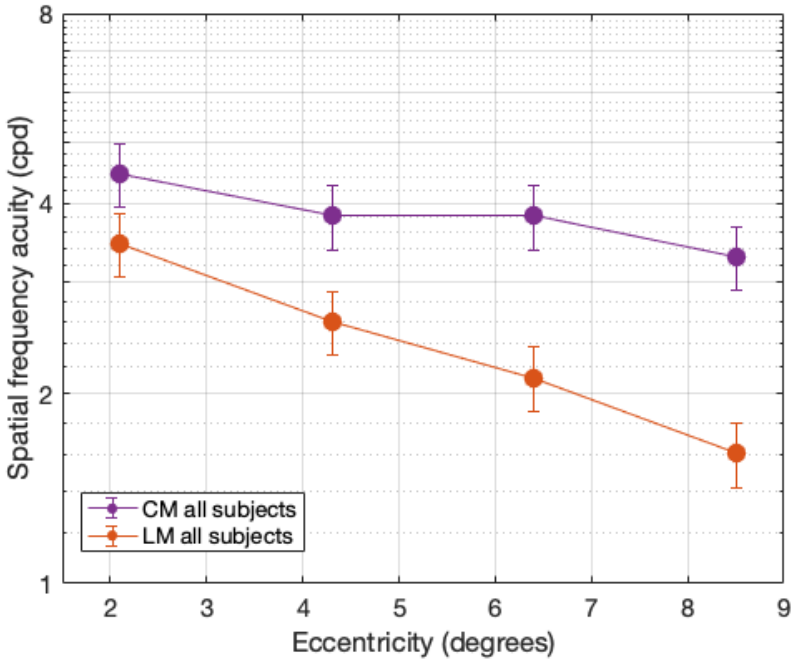

Fig. 2-7. Spatial frequency acuity (i.e. maximal spatial frequency corresponding to 75% correct) obtained through curve fitting to the high-frequency roll-off of the data in Figs. 2-5e and 2-6e, for LM (orange) and CM (purple) patterns, respectively. Error bars indicate +/- SE of mean thresholds for the N=4 observers.

2.4 Discussion

In order to translate the evidence from previous neurophysiology experiments into a human psychophysical approach, we compared the psychophysical performance for LM and CM patterns. The results of the experiments shown here indicated a likely distinct mechanism for processing LM and CM stimuli, which in particular was consistent with

neurophysiology studies where CM carrier are processed by nonlinear subunits of Y-like subcortical cells (Rosenberg et al., 2010; Rosenberg and Issa, 2011).

Spatial and temporal frequency dependence

Y-like cells such as parasol cells are characterized by their ability to respond linearly to low SF drifting gratings, and nonlinearly to high spatiotemporal frequency contrast-reversing gratings (e.g. Hochstein and Shapley, 1976; Crook et al, 2008a). In this study, we employed drifting LM stimuli at different SFs and TFs that are known to be processed by linear mechanisms, which respond best at low TF and high SF or vice versa, at high TF and low SF (e.g. Robson, 1966; Kulikowski, 1970; Watson & Ahumada, 2016). Not surprisingly, the psychophysical responses that we found for LM patterns followed this rule (Figs. 2-2,2-4). However, CM patterns are thought to be processed by nonlinear mechanisms that arise from retinal bipolar cell inputs to the Y-like ganglion cells that project to the LGN, whose responses are relayed to the visual cortex. Furthermore, the nonlinear subunits of LGN Y cells were shown to respond to relatively higher TFs compared to cortical mechanisms (Rosenberg et al., 2010; Rosenberg and Issa, 2011). Therefore, nonlinear (carrier) responses to CM patterns should be able to respond well at higher carrier spatiotemporal frequencies. This was consistent with the results in our experiments with CM patterns, where the psychophysical performance was very good at relatively high carrier SFs and high carrier TFs (Figs. 2-3,2-4). In addition, the demonstration of a bandpass dependence on carrier SF (Fig. 2-3) is consistent with similar findings for CM-responsive single neurons in early visual cortex of cats (Zhou & Baker, 1994, 1996; Tanaka & Ohzawa, 2006; Rosenberg et al, 2010; Li et al, 2014).

Eccentricity dependence

Previous human psychophysical studies using luminance gratings as a function of eccentricity demonstrated that the dependence of contrast sensitivity on SF shifts to lower SFs, with increasing eccentricity (e.g. Koenderink et al., 1977; Rovamo et al., 1978). This was true in our experiments with LM patterns (Fig.2-5). However for CM patterns, the psychophysical performance as a function of carrier SF did not shift systematically with eccentricity. This relative invariance to eccentricity for the carrier SF dependence of CM patterns might reflect the organization of the nonlinear (F2, second harmonic) receptive fields of the Y-like cells. According to primate neurophysiology studies, estimates of the center F2 receptive fields of the Y-like cells have a minimal variation with eccentricity, while the linear (F1, first harmonic) estimates of the center receptive fields decrease substantially with eccentricity (Crook et al., 2008 b).

It should be pointed out that in the experiments of Crook et al. (2008 b), the eccentricities in the primate retina used to measure F1 and F2 center receptive fields (7-40 degrees) were higher than the eccentricities (ca 2-8 deg) examined here. While it can be more challenging for inexperienced subjects to perform psychophysical judgments in more peripheral vision, it nevertheless might be worthwhile to test a higher range of eccentricities than we examined here, to provide a more direct comparison to the results of Crook et al (2008 b). According to our results and assuming that psychophysical responses to CM patterns are mediated by the nonlinear subunits of Y-like cells, the small variation in the receptive fields of F2 at different eccentricities might give rise to responses that are more constant across retinal eccentricity. While the psychophysical performance for LM patterns, mediated by linear mechanisms, might be more affected by eccentricity.

Caveats

One can argue that for our results on CM patterns, the bandpass carrier SF dependence, in particular the fall-off at low carrier SFs (Figs. 2-3, 2-6), might be secondary to a lack of a constant ratio between carrier SF and envelope SF, because envelope SF was kept at a fixed value throughout our experiments. In this case, if carrier SF and envelope SF become more similar, it might interfere with the ability to judge the direction of envelope motion as distinct from the carrier flicker, or even that there might be insufficient cycles of the carrier within each envelope cycle to provide a genuine CM pattern. However, if we had tried to keep a constant ratio, at the lowest eccentricity the visual stimulus could be so large that part of the stimulus would be overlapping the fovea and in peripheral vision it would be too small to make a reasonable judgement of motion of the envelope. Although in our experiments the ratio was not constant, we were careful to maintain a ratio of at least 3.5:1 at the lowest carrier SF, which would provide a reasonable number of carrier cycles within each cycle of the envelope, to enable judgement of the direction of envelope motion. A possible future direction to explore, to provide a potentially less difficult task for subjects, might be to employ a psychophysical task to identify the orientation of the envelope rather than its direction of motion. Because cortical neurons that encode CM stimuli are selective for orientation as well as for direction of motion of the envelope (Li et al, 2014), this approach should also be similarly specific for Y-like cells.

A natural concern when using CM patterns is that some kind of early nonlinearity, in the CRT display screen or in the photoreceptors, might act to provide an artifactual luminance signal (Baker, 1999). We performed a careful measurement of the CRT

nonlinearity, and incorporated that into the gamma correction of the video attenuator. Then we used the photometer to verify the linearity of luminance with intensity of the video signal. The visual stimuli were always displayed in the center of the CRT (where calibration for gamma correction was performed), with eccentricity being varied by placement of the fixation target rather than the stimulus. After gamma correction we also employed a diffusing sheet that acts as a spatial low-pass filter, to verify that no luminance artifact was visible, thus indicating the calibration was successful in preventing nonlinear distortions (Baker 1999; Scott-Samuel & Georgeson, 1999). To prevent possible luminance artifacts from the "adjacent pixel nonlinearity"(Schofield & Georgeson, 1999; Sukumar & Waugh, 2007), we used carrier patterns that changed luminance smoothly along the line scan of the CRT display, i.e. sinusoidal carrier waveforms. Furthermore, if the psychophysical responses to CM patterns were due to either CRT or photoreceptor nonlinearities, one would not expect a bandpass dependence on carrier spatial frequency (Figs. 2-3,2-6) - in particular, the fall-off at low carrier SFs demonstrates that the mechanism driving CM pattern responses is not secondary to simple luminance artifacts.

2.5 Conclusions

The results of this study suggest that is possible to psychophysically reflect the nonlinear responses of Y-like cells (such as parasol cells), by employing CM patterns at high spatiotemporal frequencies. With this approach, we can reveal a selective behavior of Y-like cells and separate contributions in the visual processing from other RGCs. To the

best of our knowledge, this is the first human psychophysical study that employs CM patterns at different eccentricities with the aim of isolating the function of Y-like RGCs.

Previous studies suggest that first-order stimuli which are based on variations in luminance, and second-order stimuli which are based on differences in local contrast and texture (such as CM patterns) (Cavanagh and Mather, 1989), are driven by different processing mechanisms (Cavanagh & Mather,1989; Manahilov et al., 2003; Schofield & Georgeson, 1999). Our psychophysical results using CM patterns, which are a classic second-order stimulus, suggest processing likely arising from Y-like cells which is consistent with neurophysiological evidence (Gharat and Baker, 2017; Rosenberg et al., 2010; Rosenberg and Issa, 2011). Since Y-like cells carry a mixture of first and second-order information, an important future research direction would be to explore the relationship between the mechanisms underlying responses here, and the various other psychophysical approaches that have supported either common or separate processing for first- and second-order stimuli (e.g. Allard & Faubert, 2008, 2013; Holliday & Anderson, 1994; Scott-Samuel & Georgeson, 1999; Smith & Ledgeway, 1997).

2.6 References

1. Allard R, Faubert J. First- and second-order motion mechanisms are distinct at low but common at high temporal frequencies. J Vis. 2008 Feb 28;8(2):12.1-17.

2. Allard R, Faubert J. No second-order motion system sensitive to high temporal frequencies. J Vis. 2013 Apr 4;13(5):4.

3. Baker CL Jr. Central neural mechanisms for detecting second-order motion. Curr Opin Neurobiol. 1999 Aug;9(4):461-6.

4. Brainard DH. The Psychophysics Toolbox. Spat Vis. 1997;10(4):433-6.

5. Cavanagh P, Mather G. Motion: the long and short of it. Spat Vis. 1989;4(2-3):103-29.

6. Crook JD, Peterson BB, Packer OS, Robinson FR, Gamlin PD, Troy JB, Dacey DM. The smooth monostratified ganglion cell: evidence for spatial diversity in the Y-cell pathway to the lateral geniculate nucleus and superior colliculus in the macaque monkey. J Neurosci. (2008a) Nov 26;28(48):12654-71.

7. Crook JD, Peterson BB, Packer OS, Robinson FR, Troy JB, Dacey DM. Y-cell receptive field and collicular projection of parasol ganglion cells in macaque monkey retina. J Neurosci. (2008b) Oct 29;28(44):11277-91.

8. Demb JB, Haarsma L, Freed MA, Sterling P. Functional circuitry of the retinal ganglion cell's nonlinear receptive field. J Neurosci. 1999 Nov 15;19(22):9756-67.

9. Enroth-Cugell C, Robson JG. The contrast sensitivity of retinal ganglion cells of the cat. J Physiol. 1966 Dec;187(3):517-52.

10. Gharat A, Baker CL Jr. Nonlinear Y-Like Receptive Fields in the Early Visual Cortex: An Intermediate Stage for Building Cue-Invariant Receptive Fields from Subcortical Y Cells. J Neurosci. 2017 Jan 25;37(4):998-1013.

11. Hochstein S, Shapley RM. Linear and nonlinear spatial subunits in Y cat retinal ganglion cells. J Physiol. 1976 Nov;262(2):265-84.

12. Holliday, I., & Anderson, S. Different Processes Underlie the Detection of Second Order Motion at Low and High Temporal Frequencies. Proceedings: Biological Sciences. 1994; 257(1349): 165-173.

13. Kleiner M, Brainard D, Pelli D, Ingling A, Murray R, Broussard C. What's new in psychtoolbox-3. Perception. 2007;36(14):1-16.

14. Koenderink J.J., Bouman M.A., Bueno de Mesquita A.E., Slappendel S. Perimetry of contrast detection thresholds of moving spatial sine wave patterns—I. The near peripheral visual field (eccentricity 0–8 degrees) J. opt. Soc. Am., 68 (1978), pp. 845-849.

15. Kulikowski JJ. Effective contrast constancy and linearity of contrast sensation. Vision Res. 1976;16(12):1419-31.

16. Lennie P. Perceptual signs of parallel pathways. Philos Trans R Soc Lond B Biol Sci. 1980 Jul 8;290(1038):23-37.

17. Li G, Yao Z, Wang Z, Yuan N, Talebi V, Tan J, Wang Y, Zhou Y, Baker CL Jr. Form-cue invariant second-order neuronal responses to contrast modulation in primate area V2. J Neurosci. 2014 Sep 3;34(36):12081-92.

18. Li X, Lu ZL, Xu P, Jin J, Zhou Y. Generating high gray-level resolution monochrome displays with conventional computer graphics cards and color monitors. J Neurosci Methods. 2003 Nov 30;130(1):9-18.

19. Livingstone M, Hubel D. Segregation of form, color, movement, and depth: anatomy, physiology, and perception. Science. 1988 May 6;240(4853):740-9.

20. Manahilov V, Simpson WA, Calvert J. Why is second-order vision less efficient than first-order vision? Vision Res. 2005 Oct;45(21):2759-72.

21. Merigan WH, Maunsell JH. Macaque vision after magnocellular lateral geniculate lesions. Vis Neurosci. 1990 Oct;5(4):347-52.

22. Merigan WH, Byrne CE, Maunsell JH. Does primate motion perception depend on the magnocellular pathway? J Neurosci. 1991 Nov;11(11):3422-9.

23. Pelli DG. The VideoToolbox software for visual psychophysics: transforming numbers into movies. Spat Vis. 1997;10(4):437-42.

24. Petrusca D, Grivich MI, Sher A, Field GD, Gauthier JL, Greschner M, Shlens J, Chichilnisky EJ, Litke AM. Identification and characterization of a Y-like primate retinal ganglion cell type. J Neurosci. 2007 Oct 10;27(41):11019-27.

25. Prins N, Kingdom FAA. Applying the Model-Comparison Approach to Test Specific Research Hypotheses in Psychophysical Research Using the Palamedes Toolbox. Front Psychol. 2018 Jul 23;9:1250.

26. Robson J.G. Spatial and temporal contrast sensitivity of the visual system. J. opt. Soc. Am. 1966.

27. Rosenberg A, Husson TR, Issa NP. Subcortical representation of non-Fourier image features. J Neurosci. 2010 Feb 10;30(6):1985-93.

28. Rosenberg A, Issa NP. The Y cell visual pathway implements a demodulating nonlinearity. Neuron. 2011 Jul 28;71(2):348-61.

29. Rovamo J, Virsu V, Näsänen R. Cortical magnification factor predicts the photopic contrast sensitivity of peripheral vision. Nature. 1978 Jan 5;271(5640):54-6.

30. Schiller PH, Logothetis NK, Charles ER. Role of the color-opponent and broad-band channels in vision. Vis Neurosci. 1990 Oct;5(4):321-46.

31. Shapley RM, Victor JD. How the contrast gain control modifies the frequency responses of cat retinal ganglion cells. J Physiol. 1981 Sep;318:161-79.

32. Schofield AJ, Georgeson MA. Sensitivity to modulations of luminance and contrast in visual white noise: separate mechanisms with similar behaviour. Vision Res. 1999 Aug;39(16):2697-716.

33. Smith AT, Ledgeway T. Separate detection of moving luminance and contrast modulations: fact or artifact? Vision Res. 1997 Jan;37(1):45-62.

34. Sukumar S, Waugh SJ. Separate first- and second-order processing is supported by spatial summation estimates at the fovea and eccentrically. Vision Res. 2007 Mar;47(5):581-96.

35. Tanaka H, Ohzawa I. Neural basis for stereopsis from second-order contrast cues. J Neurosci. 2006 Apr 19;26(16):4370-82.

36. Watson, Andrew & Ahumada, Albert. (2016). The pyramid of visibility. 10.2352/ISSN.2470-1173.2016.

37. Zhou Y.X, Baker C.L. Envelope-responsive neurons in areas 17 and 18 of cat. J. Neurophysiol. 1994; 72: 2134-2150.

38. Zhou Y.X, Baker C.L. Spatial properties of envelope-responsive cells in area 17 and 18 neurons of the cat.J. Neurophysiol. 1996; 75: 1038-1050.

3 Discussion and future directions

The results from the previous chapter indicate that our CM stimulus and associated behavioural task can provide a specific indication of the functioning of Y-like cells in human vision. A principal significance of this finding is that it could potentially be relevant to understanding, and perhaps the assessment of, certain kinds of visual pathology.

A number of clinical conditions have been associated with a predominant dysfunction of the magnocellular pathway, which is now thought to originate from Y-like RGCs. These conditions include neurodegenerative pathologies such as Alzheimer's disease (AD) and glaucoma, and learning disorders such as dyslexia. In AD, studies with random-dot cinematograms have found impairment in motion perception (Rizzo & Nawrot, 1998). Furthermore, the deposition of amyloid plaques and neurofibrillary tangles in the primary visual cortex is more prevalent in the M-pathway (Lennie et al., 1990). Dyslexia, a learning disability of reading and spelling with normal intellectual ability, has been associated with deficits in the magnocellular stream. These deficits are present in motion discrimination (Wilmer et al., 2004), contrast sensitivity at high temporal and low spatial frequencies (Martin and Lovegrove, 1984, 1987), and temporal processing (Laycock and Crewther, 2008). Glaucoma, a neurodegenerative disease that damages the optic nerve, has also been suggested to affect predominantly the magnocellular pathway (Quigley et al., 1987; Zhang et al., 2016). Here, we will focus on describing the evidence supporting the

deficiency of the magnocellular pathway in this disease, as well as caveats around this evidence.

Glaucoma is an optic neuropathy and a leading cause of irreversible blindness worldwide. The prevalence of glaucoma was estimated to be 76.0 million in 2020, and it is expected to increase to 111.8 million by 2040 (Tham et al., 2014). Although there are many types of glaucoma, the biggest division includes primary open angle glaucoma (POAG) and primary angle closure glaucoma (PACG). The POAG is more prevalent in Africa, while PACG is more prevalent in Asia (Tham et al., 2014). The POAG is a multifactorial progressive and chronic optic neuropathy characterized by loss of peripheral vision in early stages of the disease and followed by loss of the central visual field in later stages. It is usually bilateral, asymmetric and often affects more severely one eye before affecting the other. Increase in the intraocular pressure (IOP) is often associated to POAG and is considered its biggest risk factor. However, there are several cases of POAG with normal IOP (normal-tension glaucoma) (Mahabady et al., 2021), which is why the increase in the IOP is only considered a risk factor and not a requirement for the diagnosis of glaucoma. The common treatments for POAG consist of drugs, and laser and incisional surgery to maintain target IOP levels (Weinreb et al., 2014). Treatments based on neuroprotection of the optic nerve are also a field where considerable efforts have been made (Almasieh et al., 2010).

On the other hand, PACG is characterized by elevated IOP as a consequence of mechanical obstruction of the trabecular meshwork and subsequent impairment on the drainage of the aqueous humor (Yanoff and Duker, 2014). In this chapter we will focus on POAG.

Due to the clinical presentation of POAG, which decreases the peripheral vision in early stages and the central vision in late stages, the patients can have a poor symptomatology up to the late stages of the disease. Furthermore, even when screening test for the disease are performed on time, current psychophysical tests such as standard automated perimetry (SAP), which is the most popular functional test for glaucoma diagnosis, need a considerable loss of optic nerve fibers to show evidence of a decrease in the visual field (Quigley et al., 1982; Quigley et al., 1989). Since the outcome in patients with POAG depends on how early the disease can be detected and treated, early diagnosis is crucial for this disease.

In this chapter we will present the evidence of selective cell loss in POAG; then we will discuss clinical approaches and diagnostic tests for detection of glaucoma and we will finish this discussion with possible applications of CM patterns to selectively reflect Y-like cells (including parasol cells) function in early stages of POAG.

3.1 Selective loss of retinal ganglion cells in glaucoma

According to some studies, POAG causes earlier large diameter RGCs (Quigley et al., 1987; Quigley et al., 1988; Quigley et al., 1991). As we reviewed in the section on characterization of RGCs from Chapter 1 of this thesis, there are important differences between midget cells, parasol cells, and bistratified cells. Parasol cells are large neurons (with large dendritic fields and large axons) which project to the magnocellular layers of the LGN. They give important contributions to cortical pathways for motion perception

(Szmajda, et al., 2005) and high contrast and temporal sensitivity (Kaplan and Shapley, 1982; Leventhal et al., 1981; Perry et al., 1984). Selective lesions in the magnocellular pathway decrease the contrast sensitivity for visual stimuli at high TFs and low SFs (Merigan et al 1991 a). On the other hand, the midget RGCs project to the parvocellular layers of the LGN. They are more numerous than parasol cells, but smaller in size, with compact dendritic fields and small axons (Leventhal et al., 1981; Perry et al., 1984). They are sensitive to red-green chromatic differences, and relatively low contrast sensitivity (Derrington and Lennie., 1984; Derrington and Lennie, 1984; Kaplan and Shapley, 1982). Selective lesions in the parvocellular pathway decrease contrast sensitivity to visual stimuli at high SFs and low TFs, compromise peak visual acuity and cause a complete loss of color vision. (Merigan et al 1991 a,b; Merigan and Eskin 1986). The last main group of RGCs is the bistratified cells, also known as blue-ON/yellow-OFF (Dacey and Packer, 2003; Dacey et al.,2003, 2005) RGCs. These neurons have small cell bodies, and their main contribution is the perception of blue-yellow color vision (Martin et al.,1997; Szmajda et al.,2006; Chatterjee and Callaway, 2003). Therefore, the larger RGCs which might be affected earlier in glaucoma would correspond to parasol cells that form the magnocellular pathway.

Next, we will present different studies that support a selective cell loss in large diameter of RGCs in glaucoma. We will start with two studies of experimental models of POAG in monkeys and one experimental model in cats, both of which found a primary induced damage in RGCs at the level of the retina. We will continue with a study that found changes secondary to POAG in the LGN and end with a study that found changes related to POAG in the visual cortex.

3.1.1 Experimental models of glaucoma with selective damage in RGCs

In experiments by Quigley et al (1987), experimental POAG was induced in one eye of each of 10 monkeys. Using automated image analysis, they measured the number and diameter of the optic nerve fibers in the eye with induced glaucoma and compared these results with the fellow eye. The RGC fibers affected in the eyes with induced glaucoma had a mean diameter of 0.74 μm, while the mean diameter of the fibers in the normal fellow eyes were 0.85 μm, suggesting that the cell loss affected more large fibers. In sectors of the optic nerve, such as superior and inferior, there was atrophy of fibers of all sizes (as also seen in human eyes with glaucoma), but the large fibers had more severe damage in the same regions where smaller fibers had mild damage, suggesting that large fibers were more susceptible to glaucoma. Histopathology experiments by Glovinsky et al. (1991) also studied a model of monkeys with induced chronic glaucoma. They analyzed the diameters of the remaining RGC fibers (after a period of 6 to 24 months of induced POAG) of the experimental eye and compared them with RGC fibers of the normal fellow eye. Using histopathology, they demonstrated that large cells were more damaged than smaller cells in each of the stages of the disease (including early stages). These experiments with similar results suggested that psychophysical tests that are driven by parasol cells would be more efficient to detect POAG in the early stages while psychophysical tests for midget cells could be a good option for late stages.

Shou et al. (2003) induced experimental glaucoma in cats to determine the effects on the dendritic morphology of RGCs. By injecting endogenous ghost blood cells into the

anterior chamber of one eye, they induced elevation of the IOP from 24 to 40 mmHg. With injections of horseradish peroxidase (HRP) into layers A and A1 of the LGN, they were able to observe retrograde-label changes in the RGCs which were compared with RGCs of control animals. They analyzed cell density, body size, dendritic field radius, and number of branch bifurcations of dendrites of 720 labeled α and β RGCs. They found a significant decrease in all the parameters in the eyes with glaucoma with respect to controls. The cell loss and shrinkage of dendrites was more pronounced in α cells, than in β cells. The cell density of both α and β cells of retina and LGN declined with time and elevation of the IOP, showing a more important cell loss in large cells than in small ones. This might be explained by the effects of intraocular hypertension in the RGCs, which might cause a retinal and optic nerve ischemia with subsequent axoplasmic transport, axonal degeneration, and cell death of the RGCs (Quigley et al., 1986; Quigley et al., 1988; Quigley et al., 1987; Glovinsky et al., 1991). The anatomical and physiological difference in damage between α and β cells might favor the earlier damage of α cells. Due to their larger size and lower response thresholds, α cells might have a higher demand of oxygen and of molecules for storing and transferring energy such as adenosine triphosphate (ATP). In these experiments, they also compared to what degree α and β cells showed shrinkage in the dendritic fields; α cells had a more pronounced dendritic shrinkage than β cells, while the soma atrophy was affected in both to a similar degree. This suggests that the process of degeneration of RGCs secondary to glaucoma may originate in the dendritic arbors, continue with reduction of axon thickness and end with atrophy of the soma. Therefore, alterations in the dendritic fields might be a good sign for early diagnosis and a good point to start neuroprotection treatment; early visual evoked potentials of contrast sensitivity

function using moving gratings in peripheral retina might help to detect early changes associated to glaucoma in α cells (Shou et al., 2003).

3.1.2 Changes in LGN, SC and visual cortex associated to glaucoma

Since glaucoma is now considered a disease that affects not only the retina but the projection targets of the RGCs (LGN, SC, and visual cortex), if there is a selective loss of large diameter fibers early in the disease which correspond to parasol cells, the magnocellular pathway should be involved in this selective damage.

Using functional magnetic resonance imaging (fMRI), Zhang et al (2016) measured neural signals from the different layers of the LGN and SC, as well as from the visual cortex (V1, V2, and MT) in patients with early glaucoma. They compared their neural responses with responses in normal controls. The visual stimuli consisted of achromatic gratings for testing parasol cells (low SF sine wave gratings with contrast at 30%, and counter-phase flickering at 10 Hz) and chromatic gratings for testing midget cells (high SF, red-green square wave grating, with reversing contrast at 0.5 Hz). Compared to normal controls, patients with early glaucoma showed a reduction in the responses to achromatic visual stimuli in the magnocellular layers of the LGN and in the superficial layers of the SC. The degree of involvement in magnocellular responses in the LGN in patients with glaucoma correlated with their behavioral deficits. The patients with early glaucoma had reductions of the responses in the LGN and SC but not in the visual cortex (V1, V2, MT), which suggests that during early stages of POAG, the neuronal degeneration that is

selective for parasol cells, occurs in the subcortical visual nuclei before producing a deficit in the visual cortex. Another finding in the visual cortex of patients with early glaucoma was a slight increase in neural responses in visual cortex compared to controls. This might be related to some kind of cortical neural compensation from the glaucomatous eye, a similar mechanism to that of contrast gain control, but much longer-lasting (Zhang et al., 2016).

Yücel et al. (2003) studied the effects of glaucoma in the visual cortex. An important definition to start with is trans-synaptic (or trans-neuronal) degeneration. Trans-synaptic degeneration refers to the process by which an injury in a primary neuron (or neuron population) causes deleterious effects in distant neurons that are synaptically linked. This degeneration, which is associated with neurodegenerative diseases such as Alzheimer's disease and amyotrophic lateral sclerosis, might also be associated with glaucoma (Yücel et al., 2000; Yücel & Gupta, 2000). The experiment from Yücel et al. (2003) was based on an experimental model of POAG induced in one eye of eight monkeys for a period of 14 months. After this period, cell count and quantification of degenerative changes in cross-sectional areas of the neurons in the correspondant LGN layers was performed and compared to control animals. They observed degenerative changes in all the layers of the LGN (magnocellular, parvocellular, and koniocellular pathways) with changes that were proportional to the severity of intraocular hypertension and damage of the optic nerve. These neuropathological findings were not exclusive to the LGN layers corresponding to the glaucomatous eye but were also present in the other layers of the LGN (of the normal eye). Finally, varying degrees of loss of RGCs in the visual cortex were observed (Yücel et al., 2003).

As a whole, the experiments mentioned in this section suggest selective damage of large diameter cells (such as parasol cells) in the retina, and their projection targets in the LGN and SC, in the early stages of POAG. According to the experiments by Zhang et al (2016), the patients with early glaucoma showed a reduction of the responses in fMRI in the LGN and SC, but not in the visual cortex, suggesting that in the early stages of POAG, the neuronal degeneration that is selective for parasol cells occurs in the subcortical visual nuclei before producing a deficit in the visual cortex. Therefore, changes in the visual cortex would be presented in the late stages of POAG. These findings are consistent with the results of Yücel et al., 2003, which found changes in all the layers of the LGN and in the visual cortex. These changes are less specific, and throughout the visual pathway (including the visual cortex) which might be more representative of late stages of glaucoma than early damage.

3.2 Early detection of glaucoma

Glaucoma is a progressive disease characterized by the degeneration of the RGCs with subsequent structural changes in the optic nerve head and retina. Forming a layer in the inner retina called the retinal nerve fiber layer, the axons of the retinal ganglion cells (RGCs) converge into the optic disc (or optic nerve head), which is comprised of roughly one million fibers of RGCs. The optic disc has a pink neuro-retinal rim that corresponds to the RGCs with a central depression where the axons converge (cup). A typical clinical sign of glaucoma is the thinning of the neuroretinal rim with a subsequent enlargement of the cup (Fig. 1). After the optic disc, RGC fibers cross the barrier of the eye through the lamina

cribosa (a series of perforated connective tissues) and form the optic nerve, which then projects to the lateral geniculate nucleus (LGN) (Allingham et al., 2004).

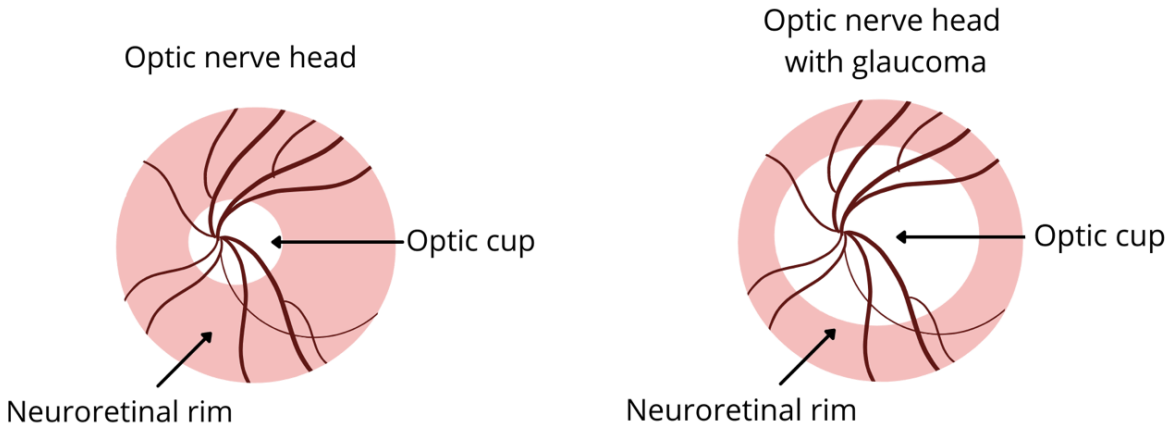

Fig. 3-1. Optic nerve head (optic disc). In the left panel, a normal optic nerve head with a proportional cup-disc ratio of approx. 0.4; the cup is the central region of the optic nerve where the axons of the RGCs converge. The neuroretinal rim corresponds to the RGCs. In the right panel, an optic disc with signs of glaucoma where the cup/disc ratio is about 0.7.

The neuronal damage in glaucoma is not limited only to the RGCs' axons in the optic nerve; it also affects neurons in the LGN (Yucel et al., 2000; Zhang et al., 2016) and the visual cortex (Gupta et al., 2006; Yucel et al., 2003). While the etiology of the loss of neurons in glaucoma is still currently unknown, the evidence points to an increase in the IOP, which alters the environment of the axons that undergo degeneration in the RGCs (Wang et al., 2002). Although in POAG there is not an obstruction in the trabecular meshwork (such as that of PACG), there is a resistance to the outflow of the aqueous humor in this region. The elevation in the IOP in POAG increases the pressure gradient across the lamina cribosa with deformation and mechanical stress of the RGCs (Bellezza et al., 2003), which leads to disruption of axonal transport and retrograde supply of

neurotrophic factors necessary for the survival of the RGCs (Burgoyne et al., 2005). The risk factors for glaucoma include being over 40 years of age, having a family history of glaucoma, being of African, Hispanic or Asian ethnicity, having high IOP, the use of corticosteroid medications, changes in the optic nerve (Fig 1), decrease in corneal thickness, previous ocular injuries, history of diabetes, migraines, high blood pressure, and circulatory problems (McMonnies, 2017).

The diagnosis of glaucoma comprises morphological changes in the optic nerve head, and the retinal nerve fiber layer (RNFL) as well as functional impairment with subsequent changes in psychophysical tests. The structural changes are detected in an exam of the eye fundus using a slit lamp and include the narrowing of the neuroretinal rim, the increase of the cup-disc ratio (Fig. 1), and changes of the RNFL (Jonas et al., 1999). When the POAG is in late stages, all these signs are clear. However, in early POAG, the diagnosis can be more challenging due to the range of variations (or appearance) in normal optic nerve heads as well as the variation of between observers in their appreciation of the optic disc (Jampel et al., 2009). There are many apparatuses currently available which support the structural and functional diagnosis of POAG. These structural devices include those for ocular imaging, where the most popular method is optical coherence tomography (OCT) that performs quantitative measures of the optic nerve head and the RFNL (Chang et al., 2009; Thatam et al., 2015). The functional tests include the standard automated perimetry (SAP), frequency doubling technology (FDT), short-wavelength automated perimetry (SWAP), and flicker-defined form perimetry (FDF) (Ramachandran, 1991). An important consideration is that the strongest diagnosis of glaucoma is when clinical, structural and functional findings are consistent with each other. For example, isolated changes in the OCT alone wouldn't be enough if there were a complete lack of functional and clinical

signs. In that case, the patient would be catalogued as a glaucoma suspect and the conduct is expectant. In this section, we will focus on the early diagnosis of glaucoma from a functional (behavioral) point of view. Recently, electrophysiological tests that are variants of the electroretinogram (ERG) such as the pattern electroretinogram (PERG), the multifocal electroretinogram (mfERG), the photopic negative response (PhNR), and the multifocal visual evoked potential (mfVEP) have been proposed as additional tools for diagnosis of glaucoma (Senger et al., 2020).

3.2.1 Standard Automated Perimetry

The SAP is the most popular psychophysical test and the current gold standard for behavioral diagnosis of POAG (Thatam et al., 2015). It uses a Humphrey perimeter with a test stimulus of 4 mm^2 and 5 different luminance magnitudes (ranging from 10,000 apostilbs (asb) to 0.1 asb). Every log order change in luminance intensity corresponds to 10 dB, resulting in measured sensitivities which can have a range over 50 dB. The SAP tests threshold values for each location of the visual field with luminance stimuli, which can be either static or kinetic. In the kinetic perimetry, the stimulus is moved at a speed of 2 to 4 degrees per second, from a subthreshold area (area of low vision) to a suprathreshold area (area of good vision), registering the point where the stimulus is detected (Johnson & Keltner, 1987). In static perimetry, the stimulus is stationary and is shown in a defined area of the visual field. The stimuli that last longer are better detected as a result of temporal summation (Allingham, et al., 2004). In the SAP, one of the most used threshold sets is the Swedish interactive threshold algorithm (SITA)-Standard 24-2, that tests the visual sensitivity at 54 locations in the central 24º of the visual field (Bengtsson et al., 1997). The

results are presented in a perimetry map showing the dB deviations from age-corrected normal sensitivities in the mentioned locations of the visual field (total deviation map); it also shows a pattern deviation map with localized scotomas after corrections for general decreases in sensitivity as well as a map reflecting the pattern deviation probability. A summary of indices including mean deviation (MD), where zero corresponds to no deviation from normal and negative values correspond to a loss of the visual field, and pattern standard deviation (PSD), which corresponds to the difference between the threshold value for each point and the average visual field sensitivity at each point (normal value for each point - the MD), are displayed in a summary of the SAP (Bengtsson et al., 1997).

Even though the SAP is considered the gold standard of behavioral tests for glaucoma, a significant loss of RGCs (of about 25-35%) may be present before showing abnormalities in this test (Kerrigan-Baumrind et al., 2000; Quigley et al., 1989; Tatham et al., 2015). Since SAP is based on a logarithmic decibel scale, it could be plausible that a considerable structural loss of RGCs in the early stages of POAG might result in minimal changes in the sensitivity of SAP (Medeiros et al., 2012). Furthermore, the overlap in the receptive fields of different RGCs in which there is some redundancy in the coverage of the retina could compensate for the deficit of a specific type of RGCs with RGCs from another population. This could be reported in the SAP as a deficit lower than the actual one (Medeiros et al., 2006). Finally, since SAP is a test that works with luminance thresholds, it is not selective for a specific type of RGC. Supposing that the early stages of POAG affect selectively parasol cells and the magnocellular pathway, SAP would have a low sensitivity for detection in early stages (Quigley et al., 1987; Quigley et al., 1988; Glovinsky et al., 1991; Shou et al., 2003; Zhang et al., 2016).

3.2.2 Frequency doubling technology

To target a specific population of RGCs, different tests such as the frequency doubling technology (FDT) were developed. The first generation FDT (Welch Allyn, Skaneateles, NY) was developed with the idea of testing the magnocellular pathway. The visual stimuli in FDT are a counterphase flickering grating at low SF and high TF. The most recent version of the FDT is the second-generation Humphrey Matrix (Carl Zeiss Meditec, Inc., Dublin, CA) which uses small targets presented along a grid. The Humphrey Matrix has different sets: 24-2, 30-2, 10-2, as well as macular threshold tests. Similar to SAP, the Humphrey Matrix provides the sensitivity across the visual field and summarizes MD and PSD. The 24-2 threshold test presents a sinusoidal grating at 5 degrees of diameter at an SF of 0.50 cpd that undergoes counterphase flicker at 18Hz (Johnson, 2008).

The FDT and the Humphrey Matrix were inspired in the frequency doubling (FD) illusion described by Kelly (1966, 1981). The FD illusion by perceived when a low SF sinusoidal grating (approximately at 4 Hz) is flickered at a high TF (approximately at 15 Hz) at a point that the SF appears to be twice the actual (physical) value. This illusion is believed to be driven by the magnocellular pathway that responds best to visual stimuli at high TF and low SF, specifically from M-y ganglion cells that were described as a nonlinear subtype of RGCs (Kelly 1981; Madess 1995, 1992). Psychophysical experiments in normal subjects by Quaid et al. (2005) found that as luminance or contrast of the stimulus is increased, its detection occurs earlier than the FD illusion. They concluded that the device for glaucoma detection (FDT) uses a counterphase flickering grating that is able to generate the FD illusion (Kelly 1966, 1981), but that the psychophysical test in the FDT is based on a flicker detection threshold, not on an FD illusion threshold (Quaid et al.,

2005). In another study that examined the mechanisms involved in the FD illusion, White et al. (2002), responses were recorded from the macaque magnocellular pathway while stimulating with counterphase-modulated sinusoidal gratings at different SFs, assessing the linearity of spatial summation. They concluded that the mechanisms of the FD illusion are caused by a cortical perception of nonlinear spatial summation, but it causes a temporal and not a spatial doubling of frequency. They suggest that the FD illusion arises from central mechanisms and not from the retina, which is consistent with results of experiments using an adaptation paradigm (Parker et al., 1981). Furthermore, White et al. (2002) concluded that the FDT test for glaucoma measures a decrease in contrast sensitivity and does not depend on the FD illusion itself. SAP and Matrix FDT have been compared to determine which is the most suited for diagnosis of POAG independently of the stages of the disease. The results between them have been similar (Spry et al., 2005). However, for early diagnosis of POAG, Matrix FDT might be superior (Liu et al., 2011; Medeiros et al., 2006).

3.2.2 Short wavelength automated perimetry and flicker-defined form perimetry

Other behavioral tests used for glaucoma diagnosis are the short wavelength automated perimetry (SWAP), also known as blue on yellow perimetry, and the flicker-defined form perimetry (FDF) (Ramachandran, 1991). The SWAP uses a chromatic (blue-violet, 440 nm wavelength) stimulus against a yellow background. This test targets bistratified cells that form the koniocellular pathway (Dacey and Lee, 1994). Since bistratified cells are a subpopulation of RGCs (5-10% of the RGC population) with little

overlap in the receptive field, SWAP is thought to be able to detect POAG earlier than other non-selective test for a subpopulation of RGCs (Tatham, 2015).

Studies that compare SAP, SWAP and FDT are controversial (Liu et al., 2011; Medeiros et al., 2006; Sample et al., 2006). The flicker defined form (FDF) (Ramachandran et al., 1991) is a stimulus in the Heidelberg edge perimeter (HEP) that measures contrast sensitivity at 54 location points (same points as for SAP 24-2). The visual stimulus consists of a phase reversal of black and white random dots at 15 Hz, which produce the percept of an illusory contour at the border of the dot area's "edge" (Mulak et al., 2012). It determines contrast thresholds for detection of the "edge", and it is inspired by second-order mechanisms that activate the magnocellular pathway (Mulak et al., 2012). Clinical studies suggest that when comparing SAP and FDF in suspected glaucoma patients, FDF might be more sensitive than SAP for early detection (Horn et al., 2014).

The early diagnosis of glaucoma is challenging. Despite having a variety of clinical, functional, and structural tests for the diagnosis of POAG, a large majority of patients are diagnosed only in later stages. It seems likely that this is due in part to the lack of symptoms in the earlier stages of the disease, a deficient screening for ocular diseases in the general population (and more important in people with risk factors for glaucoma), and low diagnostic performance of the current functional tests in the early stages of the disease. The psychophysical tests with the highest diagnostic sensitivity and specificity in early glaucoma are still a controversial topic. The development of tests with specific RGC targets, specifically parasol cells, could be useful in these early stages. In the next section, we will review the application of CM patterns as a prospective diagnostic test of glaucoma.

3.3 Use of CM patterns in glaucoma

The possibility of a selective loss of neurons of the magnocellular pathway in early glaucoma (Quigley et al., 1987; Quigley et al., 1988; Glovinsky et al., 1991; Shou et al., 2003; Zhang et al., 2016) has been an inspiration for different psychophysical tests, including the FDT and the FDF. FDT is based in the FD illusion (Kelly, 1966, 1981) and has been hypothesized to be driven by nonlinear RGCs. However, this nonlinear process in FD illusion is controversial. Furthermore, according to some authors, FDT only detects contrast sensitivity thresholds while neglecting FD thresholds (White et al., 2002). FDF is based on detection of illusory contours, a second-order stimulus (with variations in local contrast and texture) that has been shown to be processed cortically in areas V1 and V2 in cats (Zhou et al., 2001).

Visual cortex responses to CM patterns, which consist of a high SF sine wave grating carrier whose contrast is modulated by low SF sine wave envelope, have been shown by neurophysiology experiments to be driven by subcortical inputs of Y-like cells (Rosenberg et al., 2010; Rosenberg and Issa, 2011). Y-like cells are a particular type of RGC that respond linearly to low SF drifting gratings and nonlinearly to high SF contrast-reversing gratings (Hochstein and Shapley, 1976). They were first discovered in cats (Enroth-Cugell & Robson, 1966), and later the primate homologue was characterized as parasol cells (Crook et al., 2008a, b) and at least one other type of RGC (smooth/upsilon) (Petrusca et al., 2007; Crook et al., 2008a, b). Since CM pattern responses at high spatiotemporal carrier frequencies are driven by the nonlinear subunits of Y-like cells (Rosenberg et al., 2010; Rosenberg and Issa, 2011) such as parasol cells, CM patterns might be able to reveal the properties of parasol cells and the magnocellular pathway in a

more selective manner than other visual stimuli. Therefore, if there is a selective loss of neurons of the magnocellular pathway earlier in POAG (Quigley et al., 1987; Quigley et al., 1988; Glovinsky et al., 1991; Shou et al., 2003; Zhang et al., 2016), CM patterns might be able to detect this disease in these earlier stages. One future direction of this research would be to test CM patterns at high spatiotemporal carrier frequencies in patients at early stages of POAG. To elucidate the connections among the brain areas involved in visual processing of CM patterns, the psychophysical tests might be accompanied by functional magnetic resonance imaging (fMRI) scanning. In this case, if CM patterns are processed by Y-like cells such as parasol cells, we would find a dominantly a functional activation of the magnocellular pathway. Furthering this research could help provide a better understanding of how we can and hopefully one day will detect glaucoma in earlier stages.

REFERENCES

1. Almasieh M, Zhou Y, Kelly ME, Casanova C, Di Polo A. Structural and functional neuroprotection in glaucoma: role of galantamine-mediated activation of muscarinic acetylcholine receptors. Cell Death Dis. 2010;1(2):e27.
2. Allard R, Faubert J. First- and second-order motion mechanisms are distinct at low but common at high temporal frequencies. J Vis. 2008 Feb 28;8(2):12.1-17.
3. Allard R, Faubert J. No second-order motion system sensitive to high temporal frequencies. J Vis. 2013 Apr 4;13(5):4.
4. Allingham RR, Freedman S, Damji K, Shafranov G. Shield's textbook of Glaucoma, 5th edition. Lippincott Williams & Wilkins, 2004.
5. Amthor FR, Keyser KT, Dmitrieva NA. Effects of the destruction of starburst-cholinergic amacrine cells by the toxin AF64A on rabbit retinal directional selectivity. Visual Neuroscience. 2002;19:495–509.
6. Baker CL Jr. Central neural mechanisms for detecting second-order motion. Curr Opin Neurobiol. 1999 Aug;9(4):461-6.
7. Barlow HB, Levick WR. The mechanism of directionally selective units in rabbit's retina. J Physiol. 1965 Jun;178(3):477-504.
8. Blackwell R, "Contrast Thresholds of the Human Eye," J. Opt. Soc. Am. 36, 624-643 (1946)
9. Bellezza A, Rintalan C, Thompson H, Downs J, Hart R, Burgoyne R. Deformation of the lamina cribrosa and anterior scleral canal wall in early experimental glaucoma. Invest Ophthalmol Vis Sci, 44 (2003), pp. 623-637
10. Bengtsson B, Olsson J, Heijl A, Rootzén H. A new generation of algorithms for computerized threshold perimetry, SITA. Acta Ophthalmol Scand. 1997;75(4):368-75.
11. Boycott BB, Wässle H. The morphological types of ganglion cells of the domestic cat's retina. J Physiol. 1974 Jul;240(2):397-419.
12. Brainard DH. The Psychophysics Toolbox. Spat Vis. 1997;10(4):433-6.
13. Burgoyne, C.F., Downs, J.C., Bellezza, A.J., Suh, J.K., Hart, R.T. The optic nerve head as a biomechanical structure: a new paradigm for understanding the role of

IOP-related stress and strain in the pathophysiology of glaucomatous optic nerve head damage. Prog. Retin. Eye Res. 2005; 24, 39–73.

14. Cavanagh P, Mather G. Motion: the long and short of it. Spat Vis. 1989;4(2-3):103-29.
15. Cleland BG, Dubin MW, Levick WR. Sustained and transient neurones in the cat's retina and lateral geniculate nucleus. J Physiol. 1971 Sep;217(2):473-96.
16. Crook JD, Peterson BB, Packer OS, Robinson FR, Gamlin PD, Troy JB, Dacey DM. The smooth monostratified ganglion cell: evidence for spatial diversity in the Y-cell pathway to the lateral geniculate nucleus and superior colliculus in the macaque monkey. J Neurosci. (2008a) Nov 26;28(48):12654-71.
17. Crook JD, Peterson BB, Packer OS, Robinson FR, Troy JB, Dacey DM. Y-cell receptive field and collicular projection of parasol ganglion cells in macaque monkey retina. J Neurosci. (2008b) Oct 29;28(44):11277-91.
18. Chang, R.T., Knight, O.J., Feuer, W.J., Budenz, D.L., 2009. Sensitivity and specificity of timedomain versus spectral-domain optical coherence tomography in diagnosing early to moderate glaucoma. Ophthalmology 116, 2294–2299.
19. Chatterjee S, Callaway E. S cone contributions to the magnocellular visual pathway in macaque monkey. Neuron, 35 (2002), pp. 1135-1146
20. Dacey DM, Liao HW, Peterson BB, Robinson FR, Smith VC, Pokorny J, Yau KW, Gamlin PD. Melanopsin-expressing ganglion cells in primate retina signal colour and irradiance and project to the LGN. Nature. 2005;433:749–754.
21. Dacey DM, Packer OS. Colour coding in the primate retina. diverse cell types and cone-specific circuitry. Curr Opin Neurobiol. 2003;13:421–427.
22. Dacey DM, Petersen MR. Dendritic field size and morphology of midget and parasol ganglion cells of the human retina. Proc Natl Acad Sci U S A. 1992 Oct 15;89(20):9666-70.
23. Dacey DM, Peterson BB, Robinson FR, Gamlin PD. Fireworks in the primate retina: in vitro photodynamics reveals diverse LGN-projecting ganglion cell types. Neuron. 2003;37:15–27.
24. Dacey, D.M., Lee, B.B., 1994. The ‘blue-on’ opponent pathway in primate retina originates from a distinct bistratified ganglion cell type. Nature 367, 731–735.

25. Demb JB, Haarsma L, Freed MA, Sterling P. Functional circuitry of the retinal ganglion cell's nonlinear receptive field. J Neurosci. 1999 Nov 15;19(22):9756-67.
26. Demb JB, Zaghloul K, Sterling P. Cellular basis for the response to second-order motion cues in Y retinal ganglion cells. Neuron. 2001 Nov 20;32(4):711-21.
27. Derrington, A. M. and Lennie, P. (1984). Spatial and temporal contrast sensitivities of neurons in lateral geniculate nucleus of macaque. J. Physiol., 357, 219–240.
28. Enroth-Cugell C, Robson JG. The contrast sensitivity of retinal ganglion cells of the cat. J Physiol. 1966 Dec;187(3):517-52.
29. Ferster D. X- and Y-mediated synaptic potentials in neurons of areas 17 and 18 of cat visual cortex. Vis Neurosci. 1990 Feb;4(2):115-33.
30. Fukuda Y, Hsiao CF, Watanabe M. Morphological correlates of Y, X and W type ganglion cells in the cat's retina. Vision Res. 1985;25(3):319-27.
31. Gharat A, Baker CL Jr. Nonlinear Y-Like Receptive Fields in the Early Visual Cortex: An Intermediate Stage for Building Cue-Invariant Receptive Fields from Subcortical Y Cells. J Neurosci. 2017 Jan 25;37(4):998-1013.
32. Glovinsky Y, Quigley HA, Dunkelberger GR. Retinal ganglion cell loss is size dependent in experimental glaucoma. Invest Ophthalmol Vis Sci. 1991 Mar;32(3):484-91.
33. Gregg R, McCall M, Massey S. Function and anatomy of the mammalian retina. S. Ryan, A. Schachat, C. Wilkinson, D. Hinton, S. Sadda, P. Wiedemann (Eds.), Retina (fifth ed.), Elsevier, San Diego (2013), pp. 360-400.
34. Gupta N, Ang LC, Noel de Tilly L, Bidaisee L, Yucel YH (2006): Human glaucoma and neural degeneration in intracranial optic nerve, lateral geniculate nucleus, and visual cortex. Br J Ophthalmol 90:674–678.
35. Harwerth, R.S., Carter-Dawson, L., Shen, F., Smith, E.L., Crawford, M.L.. Ganglion cell losses underlying visual field defects from experimental glaucoma. Invest. Ophthalmol. Vis. Sci. (1999) 40, 2242–2250.
36. Harwerth, R.S., Carter-Dawson, L., Smith, E.L., Barnes, G., Holt, W.F., Crawford, M.L. Neural losses correlated with visual losses in clinical perimetry. Invest. Ophthalmol. Vis. Sci. (2004) 45, 3152–3160.

37. Hochstein S, Shapley RM. Linear and nonlinear spatial subunits in Y cat retinal ganglion cells. J Physiol. 1976 Nov;262(2):265-84.
38. Holliday, I., & Anderson, S. Different Processes Underlie the Detection of Second Order Motion at Low and High Temporal Frequencies. Proceedings: Biological Sciences. 1994; 257(1349): 165-173.
39. Horn, F.K., Tornow, R.P., J€unemann, A.G., Laemmer, R., Kremers, J., 2014. Perimetric measurements with flicker-defined form stimulation in comparison with conventional perimetry and retinal nerve fiber measurements. Invest. Ophthalmol. Vis. Sci. 55, 2317–2323.
40. Hubel D, Wiesel T. Receptive fields, binocular interaction and functional architecture in the cat's visual cortex. J Physiol. 1962;160(1):106-154.
41. Hubel, D. H., and T. N. Wiesel (1961) Integrative action in the cat's lateral geniculate body. J. Physiol. (Lond.) 155: 385- 398.
42. Jampel, H.D., Friedman, D., Quigley, H., Vitale, S., Miller, R., Knezevich, F., Ding, Y., 2009. Agreement among glaucoma specialists in assessing progressive disc changes from photographs in open-angle glaucoma patients. Am J. Ophthalmol. 147, 39–44.
43. Johnson CA, Keltner JL. Optimal rates of movement for kinetic perimetry. Arch Ophthalmol. 1987;105(1):73-5.
44. Johnson CA. FDT perimetry for the detection of glaucomatous visual field loss. Glaucoma Today. 2008:26-28.
45. Johnson, C.A., Adams, A.J., Casson, E.J., Brandt, J.D.. Progression of early glaucomatous visual field loss as detected by blue-on-yellow and standard white-on-white automated perimetry. Arch. Ophthalmol. (1993) 111, 651–656.
46. Jonas, J.B., Budde, W.M., Panda-Jonas, S. Ophthalmoscopic evaluation of the optic nerve head. Surv. Ophthalmol. (1999) 43, 293–320.
47. Kaplan E, Shapley RM. X and Y cells in the lateral geniculate nucleus of macaque monkeys. J Physiol (Lond). (1982) 330: 125–143
48. Kelly DH. Frequency doubling in visual responses. Journal of the Optical Society of America, 56 (1966), pp. 1628-1633

49. Kelly DH. Nonlinear visual responses to flickering sinusoidal gratings. Journal of the Optical Society of America, 71 (1981), pp. 1051-1055
50. Kerrigan-Baumrind, L.A., Quigley, H.A., Pease, M.E., Kerrigan, D.F., Mitchell, R.S., 2000. Number of ganglion cells in glaucoma eyes compared with threshold visual field tests in the same persons. Invest. Ophthalmol. Vis. Sci. 41, 741–748.
51. Kleiner M, Brainard D, Pelli D, Ingling A, Murray R, Broussard C. What's new in psychtoolbox-3. Perception. 2007;36(14):1-16.
52. Koenderink J.J., Bouman M.A., Bueno de Mesquita A.E., Slappendel S. Perimetry of contrast detection thresholds of moving spatial sine wave patterns—I. The near peripheral visual field (eccentricity 0–8 degrees) J. opt. Soc. Am., 68 (1978), pp. 845-849
53. Kolb H. Morphology and Circuitry of Ganglion Cells. 2001 May 1 [Updated 2007 Apr 4]. In: Kolb H, Fernandez E, Nelson R, editors. Webvision: The Organization of the Retina and Visual System [Internet]. Salt Lake City (UT): University of Utah Health Sciences Center; 1995
54. Kuffler, S. W. (1952) Neurons in the retina: Organization, inhibition and excitation problems. Cold Spring Harbor Symp. Quant. Biol. 17: 281-292.
55. Kulikowski JJ. Effective contrast constancy and linearity of contrast sensation. Vision Res. 1976;16(12):1419-31.
56. Landers, J.A., Goldberg, I., Graham, S.L., 2003. Detection of early visual field loss in glaucoma using frequency-doubling perimetry and short-wavelength automated perimetry. Arch. Ophthalmol. 121, 1705–1710.
57. Lennie P. Perceptual signs of parallel pathways. Philos Trans R Soc Lond B Biol Sci. 1980 Jul 8;290(1038):23-37.
58. Lennie, P. (1980). Parallel visual pathways: A review. Vision Research, 20, 561-594.
59. Leventhal AG, Rodieck RW, Dreher B. Retinal ganglion cell classes in the old world monkey: Morphology and central projections. Science (1981) 213:1139 – 1142.

60. Li G, Yao Z, Wang Z, Yuan N, Talebi V, Tan J, Wang Y, Zhou Y, Baker CL Jr. Form-cue invariant second-order neuronal responses to contrast modulation in primate area V2. J Neurosci. 2014 Sep 3;34(36):12081-92.
61. Li X, Lu ZL, Xu P, Jin J, Zhou Y. Generating high gray-level resolution monochrome displays with conventional computer graphics cards and color monitors. J Neurosci Methods. 2003 Nov 30;130(1):9-18.
62. Liu, S., Lam, S., Weinreb, R.N., Ye, C., Cheung, C.Y., Lai, G., Lam, D.S., Leung, C.K. Comparison of standard automated perimetry, frequency-doubling technology perimetry, and short-wavelength automated perimetry for detection of glaucoma. Invest. Ophthalmol. Vis. Sci. (2011) 52, 7325–7331.
63. Livingstone M, Hubel D. Segregation of form, color, movement, and depth: anatomy, physiology, and perception. Science. 1988 May 6;240(4853):740-9.
64. Maddess T, Henry G. Nonlinear visual responses and visual deficits in ocular hypertensive and glaucoma subjects. Clinical and Visual Science, 7 (1992), pp. 371-383.
65. Maddess, T. (1995). Early detection of glaucoma. USA, Patent No. 5912723.
66. Mahabadi N, Foris LA, Tripathy K. Open Angle Glaucoma. [Updated 2021 Feb 14]. In: StatPearls [Internet]. Treasure Island (FL): StatPearls Publishing; 2021 Jan-.
67. Manahilov V, Simpson WA, Calvert J. Why is second-order vision less efficient than first-order vision? Vision Res. 2005 Oct;45(21):2759-72.
68. Mareschal I, Baker CL Jr (1998) Temporal and spatial response to second order stimuli in cat A18. J Neurophysiol 80:2811–282.
69. Martin P., White A., Goodchild A., Wilder H, Sefton A. Evidence that blue-on cells are part of the third geniculocortical pathway in primates European Journal of Neuroscience, 9 (1997), pp. 1536-1541
70. Masland RH. The fundamental plan of the retina. Nat Neurosci. 2001 Sep;4(9):877-86.
71. Masland RH. The neuronal organization of the retina. Neuron. 2012 Oct 18;76(2):266-80.
72. McMonnies CW. Glaucoma history and risk factors. J Optom. 2017 Apr-Jun;10(2):71-78.

73. Medeiros, F.A., Sample, P.A., Zangwill, L.M., Liebmann, J.M., Girkin, C.A., Weinreb, R.N. A statistical approach to the evaluation of covariate effects on the receiver operating characteristic curves of diagnostic tests in glaucoma. Invest. Ophthalmol. Vis. Sci.(2006) 47, 2520–2527.
74. Medeiros, F.A., Zangwill, L.M., Bowd, C., Mansouri, K., Weinreb, R.N., 2012. The structure and function relationship in glaucoma: implications for detection of progression and measurement of rates of change. Invest. Ophthalmol. Vis. Sci. 53, 6939–6946.
75. Merigan WH, Byrne CE, Maunsell JH. Does primate motion perception depend on the magnocellular pathway? J Neurosci. 1991 Nov;11(11):3422-9.
76. Merigan WH, Maunsell JH. Macaque vision after magnocellular lateral geniculate lesions. Vis Neurosci. 1990 Oct;5(4):347-52.
77. Merigan, W. H., & Eskin, T. A. Spatio-temporal vision of macaques with severe loss of retinal ganglion cells. Vision Research, (1986); 26(11), 1751–1761.
78. Merigan, W.H.(1991). P and M pathway specializations in the Macaque. In Valberg, A. & Lee, B.B. (Eds), From pigments to perception 117-125. New York: Plenum Press.
79. Molday RS, Moritz OL. Photoreceptors at a glance. J Cell Sci. 2015 Nov 15;128(22):4039-45.
80. Mulak M, Szumny D, Sieja-Bujewska A, Kubrak M. Heidelberg edge perimeter employment in glaucoma diagnosis--preliminary report. Adv Clin Exp Med. 2012 Sep-Oct;21(5):665-70.
81. Nelson R, Connaughton V. Bipolar Cell Pathways in the Vertebrate Retina. 2007 May 24 [updated 2012 Jan 20]. In: Kolb H, Fernandez E, Nelson R, editors. Webvision: The Organization of the Retina and Visual System [Internet]. Salt Lake City (UT): University of Utah Health Sciences Center; 1995.
82. Parker A. Shifts in perceived periodicity induced by temporal modulation and their influence on the spatial frequency tuning of two aftereffects. Vision Res. 1981;21:1739–1747.
83. Pelli DG. The VideoToolbox software for visual psychophysics: transforming numbers into movies. Spat Vis. 1997;10(4):437-42.

84. Pelli, D. G., & Zhang, L. (1991). Accurate control of contrast on microcomputer displays. Vision Research, 31*(7-8)*, 1337–1350.
85. Perry, V. H., Oehler, R. and Cowey, A. (1984). Retinal ganglion cells which project to the dorsal lateral geniculate nucleus in the macaque monkey.. Neuroscience, 12, 1101–1123.
86. Petrusca D, Grivich MI, Sher A, Field GD, Gauthier JL, Greschner M, Shlens J, Chichilnisky EJ, Litke AM. Identification and characterization of a Y-like primate retinal ganglion cell type. J Neurosci. 2007 Oct 10;27(41):11019-27.
87. Prins N, Kingdom FAA. Applying the Model-Comparison Approach to Test Specific Research Hypotheses in Psychophysical Research Using the Palamedes Toolbox. Front Psychol. 2018 Jul 23;9:1250.
88. Purves D, Augustine GJ, Fitzpatrick D, et al., editors. Neuroscience. 2nd edition. Sunderland (MA): Sinauer Associates; 2001.
89. Quigley HA, Addicks EM, and Green WR: Optic nerve damage in human glaucoma: III. Quantitative correlation of nerve fiber loss and visual field defect in glaucoma, ischemic neuropathy, disc edema, and toxic neuropathy. Arch Ophthalmol 100:135, 1982.
90. Quigley HA, Dunkelberger GR, and Green WR: Chronic human glaucoma causes selectively greater loss of large optic nerve fibers. Ophthalmology (1988); 95:357.
91. Quigley HA, Sanchez RM, Dunkelberger GR, L'Hernault NL, and Baginski TA: Chronic glaucoma selectively damages large optic nerve fibers. Invest Ophthalmol Vis Sci 28:913, 1987.
92. Quigley HA. Pathophysiology of the optic nerve in glaucoma. In: McAllister JA, Wilson RP, eds. Glaucoma. London: Butterworth; 1986:30–53.
93. Ramachandran, V.S., Rogers-Ramachandran, D.C. Phantom contours: A new class of visual patterns that selectively activates the magnocellular pathway in man. Bull. Psychon. Soc. 29, 391–394 (1991).
94. Robson J.G. Spatial and temporal contrast sensitivity of the visual system. J. opt. Soc. Am. 1966.
95. Rodieck R. Annual Review of Neuroscience 1979 2:1, 193-225

96. Rosenberg A, Husson TR, Issa NP. Subcortical representation of non-Fourier image features. J Neurosci. 2010 Feb 10;30(6):1985-93.
97. Rosenberg A, Issa NP. The Y cell visual pathway implements a demodulating nonlinearity. Neuron. 2011 Jul 28;71(2):348-61.
98. Rosenberg A, Talebi V. The primate retina contains distinct types of Y-like ganglion cells. J Neurosci. 2009 Apr 22;29(16):5048-50.
99. Rovamo J, Virsu V, Näsänen R. Cortical magnification factor predicts the photopic contrast sensitivity of peripheral vision. Nature. 1978 Jan 5;271(5640):54-6.
100. Sample, P.A., Medeiros, F.A., Racette, L., Pascual, J.P., Boden, C., Zangwill, L.M., Bowd, C., Weinreb, R.N. Identifying glaucomatous vision loss with visual-function–specific perimetry in the diagnostic innovations in glaucoma study. Invest. Ophthalmol. Vis. Sci. (2006) 47, 3381–3389.
101. Scott-Samuel NE, Georgeson MA. Feature matching and segmentation in motion perception. Proc Biol Sci. 1999 Nov 22;266(1435):2289-94.
102. Schiller PH, Logothetis NK, Charles ER. Role of the color-opponent and broad-band channels in vision. Vis Neurosci. 1990 Oct;5(4):321-46.
103. Schofield AJ, Georgeson MA. Sensitivity to modulations of luminance and contrast in visual white noise: separate mechanisms with similar behaviour. Vision Res. 1999 Aug;39(16):2697-716.
104. Senger C, Moreto R, Watanabe SES, Matos AG, Paula JS. Electrophysiology in Glaucoma. J Glaucoma. 2020 Feb;29(2):147-153.
105. Shapley RM, Victor JD. How the contrast gain control modifies the frequency responses of cat retinal ganglion cells. J Physiol. 1981 Sep;318:161-79.
106. Shapley, R. and Perry, V. H. (1986). Cat and monkey retinal ganglion cells and their visual functional roles. Trends in NeuroSciences, 9(5), 229–235.
107. Shapley. R. M. & Victor. J. D. (1981). How the contrast gain control modifies the frequency responses of cat retinal ganglion cells. Journal of Physiology. 318. I61 -179.
108. Shou T, Liu J, Wang W, Zhou Y, Zhao K. Differential dendritic shrinkage of alpha and beta retinal ganglion cells in cats with chronic glaucoma. Invest Ophthalmol Vis Sci. 2003 Jul;44(7):3005-10

109. Smith AT, Ledgeway T. Separate detection of moving luminance and contrast modulations: fact or artifact? Vision Res. 1997 Jan;37(1):45-62.

110. Spry, P.G., Hussin, H.M., Sparrow, J.M., 2005. Clinical evaluation of frequency doubling technology perimetry using the Humphrey Matrix 24–2 threshold strategy. Br. J. Ophthalmol. 89, 1031–1035.

111. Sukumar S, Waugh SJ. Separate first- and second-order processing is supported by spatial summation estimates at the fovea and eccentrically. Vision Res. 2007 Mar;47(5):581-96.

112. Szmajda B, Buzás P, FitzGibbon T, Martin P. Geniculocortical relay of blue-off signals in the primate visual system. Proceedings of the National Academy of Sciences of the United States of America, 103 (2006), pp. 19512-19517.

113. Szmajda BA, Grünert U, Martin PR. Mosaic properties of midget and parasol ganglion cells in the marmoset retina. Vis Neurosci. 2005 Jul-Aug;22(4):395-404.

114. Tanaka H, Ohzawa I. Neural basis for stereopsis from second-order contrast cues. J Neurosci. 2006 Apr 19;26(16):4370-82.

115. Tatham AJ, Medeiros FA, Zangwill LM, Weinreb RN. Strategies to improve early diagnosis in glaucoma. Prog Brain Res. 2015;221:103-33.

116. Tham YC, Li X, Wong TY, Quigley HA, Aung T, Cheng CY. Global prevalence of glaucoma and projections of glaucoma burden through 2040: a systematic review and meta-analysis. Ophthalmology. 2014 Nov;121(11):2081-90.

117. To L, Woods RL, Goldstein RB, Peli E. Psychophysical contrast calibration. Vision Res. 2013;90:15-24.

118. Twig, G., Levy, H., and Perlman, I. (2003). Color opponency in horizontal cells of the vertebrate retina. Prog. Retin. Eye Res. 22, 31–68.

119. Watson, Andrew & Ahumada, Albert. (2016). The pyramid of visibility. 10.2352/ISSN.2470-1173.2016.

120. Wensel TG (2012) Molecular biology of vision. In: Brady ST, Albers RW, Price D, Siegel JG (Eds.) Basic neurochemistry: principles of molecular, cellular, and medical neurobiology, 8th edn. Elsevier, London, pp 889–903

121. Weinreb RN, Aung T, Medeiros FA. The pathophysiology and treatment of glaucoma: a review. JAMA. 2014 May 14;311(18):1901-11.

122. Werblin, F.S. and J.E. Dowling, Organization of the retina of the mudpuppy, Necturus maculosus. II. Intracellular recording. J Neurophysiol, 1969. 32(3): p. 339-55.

123. White, A.J., Sun, H., Swanson, W.H., Lee, B.B. An examination of physiological mechanisms underlying the frequency-doubling illusion. Invest. Ophthalmol. Vis. Sci. (2002) 43, 3590–3599.

124. Wilson, P. D., M. H. Rowe, and J. Stone (1976) Properties of relay cells in the cat's lateral geniculate nucleus: A comparison of W-cells with X- and Y-cells. J. Neurophysiol. 39: 1193-1209.

125. Yanoff, M., & Duker, J. S. (Eds.). (2019). Ophthalmology (Fifth). Elsevier Saunders.

126. YH Yucel, Q Zhang, N Gupta, PL Kaufman, RN Weinreb. Loss of neurons in magnocellular and parvocellular layers of the lateral geniculate nucleus in glaucoma. Arch Ophthalmol, 118 (2000), pp. 378-384

127. YH Yucel, Q Zhang, RN Weinreb, PL Kaufman, N Gupta. Effects of retinal ganglion cell loss on magno-, parvo-, koniocellular pathways in the lateral geniculate nucleus and visual cortex in glaucoma. Prog Retin Eye Res, 22 (2003), pp. 465-481

128. Yoshida K, Watanabe D, Ishikane H, Tachibana M, Pastan I, Nakanishi S. A key role of starburst amacrine cells in originating retinal directional selectivity and optokinetic eye movement. *Neuron.* 2001;30:771–780.

129. Zhang P, Wen W, Sun X, He S. Selective reduction of fMRI responses to transient achromatic stimuli in the magnocellular layers of the LGN and the superficial layer of the SC of early glaucoma patients. Hum Brain Mapp. 2016 Feb;37(2):558-69.

130. Zhou Y, Jia F, Tao H, Shou T. The responses to illusory contours of neurons in cortex areas 17 and 18 of the cats. Sci China C Life Sci. 2001 Apr;44(2):136-45.

131. Zhou Y.X, Baker C.L. Envelope-responsive neurons in areas 17 and 18 of cat. J. Neurophysiol. 1994; 72: 2134-2150.

132. Zhou Y.X, Baker C.L. Envelope-responsive neurons in areas 17 and 18 of cat. J. Neurophysiol. 1994; 72: 2134-2150.

133. Zhou Y.X, Baker C.L. Spatial properties of envelope-responsive cells in area 17 and 18 neurons of the cat.J. Neurophysiol. 1996; 75: 1038-1050.